CENTER FOR INFRASTRUCTURE ENGINEERING STUDIES

In-situ load testing of Bridge A6358 Osage Beach, MO

By

Fabio Matta

Filippo Bastianini

Nestore Galati

Paolo Casadei

and

Antonio Nanni

University Transportation Center Program at
The University of Missouri-Rolla

UTC
R124-3

Disclaimer

The contents of this report reflect the views of the author(s), who are responsible for the facts and the accuracy of information presented herein. This document is disseminated under the sponsorship of the Department of Transportation, University Transportation Centers Program and the Center for Infrastructure Engineering Studies UTC program at the University of Missouri - Rolla, in the interest of information exchange. The U.S. Government and Center for Infrastructure Engineering Studies assumes no liability for the contents or use thereof.

Technical Report Documentation Page

1. Report No.	2. Government Accession No.	3. Recipient's Catalog No.
UTC R124-3		

4. Title and Subtitle	5. Report Date
In-situ load testing of Bridge A6358 Osage Beach, MO	January 2005
	6. Performing Organization Code

7. Author/s	8. Performing Organization Report No.
F. Matta, F. Bastianini, N. Galati, P. Casadei, and A. Nanni	00001104

9. Performing Organization Name and Address	10. Work Unit No. (TRAIS)
Center for Infrastructure Engineering Studies/UTC program University of Missouri - Rolla 223 Engineering Research Lab Rolla, MO 65409	11. Contract or Grant No. DTRS98-G-0021

12. Sponsoring Organization Name and Address	13. Type of Report and Period Covered
U.S. Department of Transportation Research and Special Programs Administration 400 7th Street, SW Washington, DC 20590-0001	Final
	14. Sponsoring Agency Code

15. Supplementary Notes

16. Abstract

This report presents the assessment of a High Performance Steel (HPS) bridge located at the Lake of the Ozarks in Miller County, MO. The bridge number is A6358 and it is located on US Rt. 54/Osage River. Two different modern techniques for Structural Health Monitoring (SHM) were applied for this purpose, in order to advance their field validation process.

Displacements of the girders during the pouring of the concrete deck and a diagnostic load test, conducted after the bridge completion, were evaluated using an optical non-contact measurement technique based on an automated total station system. The setup included a total of 22 reflecting prisms mounted onto the bottom flange of the girders, plus four reference targets placed outside the bridge superstructure.

Strain and temperature distributions along some of the girders were measured during the diagnostic load test using a fiber optic distributed Brillouin sensing technique. The method is based on the “Brillouin” phenomenon, which defines a linear relation between the axial strain in an optical fiber, and the corresponding shift in the frequency distribution of the scattered Brillouin light generated when an optical impulse runs through a fiber. A single optical circuit, comprised of bare fibers and a custom-made novel glass FRP tape with embedded sensing fibers, was installed on the web of the girders at different depths, along two continuous spans.

17. Key Words	18. Distribution Statement
Assessment, bridge monitoring, concrete deck, fiber optics, high performance steel, in-situ load test,	No restrictions. This document is available to the public through the National Technical Information Service, Springfield, Virginia 22161.

19. Security Classification (of this report)	20. Security Classification (of this page)	21. No. Of Pages	22. Price
Unclassified	Unclassified		

Form DOT F 1700.7 (8-72)

RESEARCH INVESTIGATION RI04-004

IN-SITU LOAD TESTING OF BRIDGE A6358
OSAGE BEACH, MO

PREPARED FOR THE

MISSOURI DEPARTMENT OF TRANSPORTATION

IN COOPERATION WITH THE

UNIVERSITY TRANSPORTATION CENTER

Written by:

Fabio Matta, Graduate Research Assistant at UMR
Filippo Bastianini, Adjunct Assistant Professor at UMR
Nestore Galati, Research Engineer at UMR
Paolo Casadei, Research Engineer at SGM S.r.l., San Mariano (PG) - Italy
Antonio Nanni, V. & M. Jones Professor of Civil Engineering

CENTER FOR INFRASTRUCTURE ENGINEERING STUDIES
UNIVERSITY OF MISSOURI – ROLLA

Submitted
January 2005

IN-SITU LOAD TESTING OF BRIDGE A6358

OSAGE BEACH, MO

EXECUTIVE SUMMARY

This report presents the assessment of a High Performance Steel (HPS) bridge located at the Lake of the Ozarks in Miller County, MO. The bridge number is A6358 and it is located on US Rt. 54/Osage River. Two different modern techniques for Structural Health Monitoring (SHM) were applied for this purpose, in order to advance their field validation process.

Displacements of the girders during the pouring of the concrete deck and a diagnostic load test, conducted after the bridge completion, were evaluated using an optical non-contact measurement technique based on an automated total station system. The setup included a total of 22 reflecting prisms mounted onto the bottom flange of the girders, plus four reference targets placed outside the bridge superstructure.

Strain and temperature distributions along some of the girders were measured during the diagnostic load test using a fiber optic distributed Brillouin sensing technique. The method is based on the "Brillouin" phenomenon, which defines a linear relation between the axial strain in an optical fiber, and the corresponding shift in the frequency distribution of the scattered Brillouin light generated when an optical impulse runs through a fiber. A single optical circuit, comprised of bare fibers and a custom-made novel glass FRP tape with embedded sensing fibers, was installed on the web of the girders at different depths, along two continuous spans.

Experimental deflection and strain data were verified to be consistent with each other and allowed to evaluate the actual girder distribution factors. The comparison between experimental and theoretical results based on the AASHTO LRFD Bridge Design Specifications (AASHTO, 1998) allowed establishing the safety of the structure, although pointing out a significant drop in the expected behavior of one of the external girders, which may call for further assessment.

ACKNOWLEDGMENTS

The project was made possible with the financial support received from the Missouri Department of Transportation (MoDOT), and the University Transportation Center (UTC) on Advanced Materials. Several people and parties actively participated:

- Mr. John Wenzlick and Mr. Rick Simmons (MoDOT), in organizing and performing the load tests;
- Leica Geosystems, in particular in the persons of Mr. Gerard Manley and Mr. Jim Naismith, in the setup of the automated total station surveying system and providing assistance during the load test;
- Pirelli Cavi e Sistemi S.p.A., in particular in the person of Dr. Enrico Consonni, by donating the optical fibers;
- Rocafix/Isaberg Rapid Group, in particular in the person of Mr. Fabio Ruggeri, by donating the low temperature glue;
- Yokogawa Corporation of America, Test & Measurement Division/ANDO Product Group, in particular in the person of Dr. Nobuyuki Morita, in the cooperation and efforts to make the strain analyzer unit available;
- SEAL S.p.A. (SAATI Group), and in particular Mr. Paolo Grati, in manufacturing the custom-made smart GFRP tape;
- Rolla Technical Institute (RTI), in particular in the persons of Mr. Max Vath, the personnel and students of the Machine Technology and Precision Manufacturing, in the design and construction of the modular cart;
- Strongwell, in particular in the person of Mr. Richard Altice, by donating the GFRP pultruded structural panels used in the modular cart.

All of these precious contributions are gratefully acknowledged.

TABLE OF CONTENTS

EXECUTIVE SUMMARY IV
ACKNOWLEDGMENTS V
TABLE OF CONTENTS VI
LIST OF FIGURES VIII
LIST OF TABLES XI
NOTATIONS XII
1. INTRODUCTION 1
1.1 Background 1
1.1.1 Historical background on high performance steel bridges 1
1.1.2 Live-load deflections 2
1.1.3 Diagnostic load testing 2
1.2 Bridge description 3
1.3 Objectives 3
1.4 Methodology 5
1.5 Description of measurement technologies 6
1.5.1 Automated Total Station system for deflection measurement 6
1.5.2 Brillouin Optical Time-Domain Reflectometry for strain distribution measurement 7
1.5.2.1 Theoretical foundations 7
1.5.2.2 Practical applications 9
1.5.2.3 Sensing fibers and smart FRP tape 11
1.5.3 Data Acquisition System 11
2. ATS BASED DISPLACEMENT MEASUREMENT: FIELD EVALUATION 13
2.1 Bridge instrumentation 13
2.2 Deck installation 14
2.2.1 Test procedure 14
2.2.2 Test results 14
2.2.3 Discussion of results 16
2.3 Load test 21
2.3.1 Test procedure 21
2.3.2 Test results 23
2.3.3 Discussion of results 26
3. BOTDR BASED STRAIN MEASUREMENT: FIELD EVALUATION 32
3.1 Bridge instrumentation 32
3.1.1 Installation of optical fibers 32

3.1.2 Modular cart for sensor installation 35
3.1.3 Connection and preliminary testing of the sensing elements 36
3.1.4 Sensing system calibration 38
3.1.5 Installation of resistive strain gauges 39
3.2 Test procedure 40
3.3 Test results 41
3.3.1 BOTDR strain measurement 41
3.3.2 Resistive strain gauge measurements 44
3.4 Discussion of results 44
4. CONCLUSIONS 51
5. REFERENCES 52
APPENDIX I – LOAD TEST STOPS 55
APPENDIX II – RAW DATA 57
II.a Deflection data (ATS) 57
II.b Strain data (BOTDR) 59

LIST OF FIGURES

Figure 1 – Bridge A6358, U.S. Rt. 54/Osage River, Lake of the Ozarks, Miller County, MO..... 3
Figure 2 – Bridge details (not to scale)..... 4
Figure 3 – Framing plan (not to scale, all dimensions in mm)..... 5
Figure 4 – ATR TS system equipment for non-contact deflection measurement..... 6
Figure 5 – Representation of quantum energy level of Brillouin scattering process showing both Stokes (left) and anti-Stokes (right) collisions..... 8
Figure 6 – simplified schematic diagram of self-heterodyne BOTDR..... 9
Figure 7 – Schematic of correlation between elapsed time (*T*) and scanned length (*l*)..... 9
Figure 8 – Brillouin OTDR..... 9
Figure 9 – Brillouin technology for structural monitoring..... 10
Figure 10 – Smart GFRP tape..... 11
Figure 11 – Portable data acquisition system ("Orange Box")..... 12
Figure 12 – Target positions: plan view (not to scale, all dimensions in ft)..... 13
Figure 13 – Reflecting prisms mounted on steel I-girders..... 13
Figure 14 – Pouring of concrete deck and deflection measurement *via* ATS..... 14
Figure 15 – Progression of deck pouring at deflection measurement steps..... 14
Figure 16 – Measured longitudinal deflections (deck pouring, Girder 1)..... 15
Figure 17 – Measured longitudinal deflections (deck pouring, Girder 3)..... 15
Figure 18 – Measured longitudinal deflections (deck pouring, Girder 5)..... 16
Figure 19 – Measured transversal deflections (deck pouring)..... 16
Figure 20 – Comparison between theoretical and experimental longitudinal deflections (deck pouring, Girder 1)..... 18
Figure 21 – Comparison between theoretical and experimental longitudinal deflections (deck pouring, Girder 3)..... 19
Figure 22 – Comparison between theoretical and experimental longitudinal deflections (deck pouring, Girder 5)..... 20
Figure 23 – Dump trucks used for load test..... 21
Figure 24 – Transverse position of trucks during load test (not to scale)..... 22
Figure 25 – Total station in load test configuration..... 23
Figure 26 – Experimental longitudinal deflection (load test, Girder 1)..... 23
Figure 27 – Experimental longitudinal deflections (load test, Girder 3)..... 24

Figure 28 – Experimental longitudinal deflections (load test, Girder 5) 24
Figure 29 – Experimental transversal deflections at midspan of Span 1 (load test) 25
Figure 30 – Experimental deflections for Girder 1, Stop 8 and Girder 5, Stop 6 (load test) 25
Figure 31 – Girder 1 fallen due to wind during erection of bridge superstructure 26
Figure 32 – Comparison between AASHTO provisions and experimental longitudinal deflections (load test, Girder 1) 28
Figure 33 – Comparison between AASHTO provisions and experimental longitudinal deflections (load test, Girder 5) 29
Figure 34 – Comparison between AASHTO and experimental girder load distribution factor at midspan between Abutment 1 and Pier 2 in case of one lane loaded (Stop 3, 4, 5, 6 and 8) 30
Figure 35 – Comparison between AASHTO and experimental girder load distribution factor at midspan between Abutment 1 and Pier 2 in case of two lanes loaded (Stop 1, 2 and 7) 30
Figure 36 – Schematic of fiber circuit placement 32
Figure 37 – Detailed location of fiber optics on girder web (not to scale, dimensions in in) 33
Figure 38 – Smart FRP installed on Girder 1 and folded at Pier 2 location to extend circuit 34
Figure 39 – Sensing fibers installed onto web plate of Girder 2 35
Figure 40 – Sensing fibers installed onto web plate of Girder 5 35
Figure 41 – Modular frame cart for sensor installation 36
Figure 42 – Optical fiber core-alignment fusion splicing field operation 37
Figure 43 – Optical loss measured along sensing circuit 37
Figure 44 – Strain calibration fixture 38
Figure 45 – Linearity of measured and imposed strain for different fibers tested 39
Figure 46 – Strain-temperature correlation 39
Figure 47 – Close-up of strain gauges installed on top flange of Girder 1 40
Figure 48 – Field equipment for distributed strain measurement 41
Figure 49 – Proprietary software for strain data processing 41
Figure 50 – Experimental strain distribution (Stop 1) 42
Figure 51 – Experimental strain distribution (Stop 2) 42
Figure 52 – Experimental strain distribution onn Girder 5 (Stop 4) 42
Figure 53 – Experimental strain distribution (Stop 7) 43
Figure 54 – Experimental strain distribution on Girder 1 and Girder 2 (Stop 8) 43
Figure 55 – Time history of strain gauge readings 44
Figure 56 – Strain gauge data computed for Stop 1-8 accounting for thermal compensation 44
Figure 57 – Comparison between experimental and predicted strain profiles (Stop 1) 45

Figure 58 – Comparison between experimental and predicted strain profiles (Stop 2)..... 46
Figure 59 – Comparison between experimental and predicted strain profiles (Stop 4)..... 47
Figure 60 – Comparison between experimental and predicted strain profiles (Stop 7)..... 48
Figure 61 – Comparison between experimental and predicted strain profiles (Stop 8)..... 49

LIST OF TABLES

Table 2.1 – Properties of steel girder sections (as in Figure 2b) for deflection computation during deck pouring 17

Table 2.2 – Dump trucks used for load test: weight distribution assumed for analysis 21

Table 2.3 – GDFs as per AASHTO LRFD Bridge Design Specifications (1998) 26

Table 2.4 – Input data for calculation of GDFs (AASHTO, 1998) 27

Table 3.1 – Properties of Wabo MBrace saturant for fiber optics installation (Wabo, 2004) 32

Table 3.2 – Type, identification and location of sensing elements installed 33

Table 3.3 – Type, identification and location of strain gauges installed 40

NOTATIONS

A_s	:	Area of steel girder section
A_b	:	Cross sectional area of concrete barrier
E_c	:	Modulus of elasticity of concrete
E_s	:	Modulus of elasticity of steel
I_s	:	Moment of inertia of steel girder section
K_g	:	Longitudinal stiffness parameter
L	:	Span length
M_p	:	Plastic moment capacity
M_y	:	Yield moment capacity
P_1	:	Dump truck front axle load
P_2	:	Dump truck rear axle load
S	:	Girder spacing
e_g	:	Distance between center of gravity of girder section and concrete deck
f_y	:	Steel yield strength
h_{web}	:	Clear distance between flanges of I-girder
hv_a	:	Energy transfer to/from acoustic phonon
m	:	Multiple presence factor
t_c	:	Thickness of concrete deck
$w_{overhang}$	:	Overhang width from exterior girder center line
δ_i	:	Deflection of ith girder at surveying prism location
v_0	:	Frequency of monocromatic light source
v_a	:	Frequency shift of scattered phonons

1. INTRODUCTION

1.1 Background

1.1.1 Historical background on high performance steel bridges

Collaboration between government and industry has led to the development of high performance steel (HPS) for bridge applications. HPS offers increased yield strength, enhanced weldability, and improved toughness, and it may lead to lighter and more economical structures. The introduction of High Performance Steel (HPS) with minimum yield strength of 70 ksi (HPS 70W) in 1994 and its utilization in bridge design and construction coincided with various design limitations imposed by the AASHTO Standard Specifications (AASHTO, 1996). At the time, these limitations reflected the lack of test data to fully comprehend the behavior of bridges constructed using HPS. The code limitations were addressed through multiple research projects funded by the HPS steering committee and the Federal Highway Administration (FHWA). As a result, a coordinated national effort was initiated by the steel industry to address these limitations. The effort was coordinated by the American Iron and Steel Institute's (AISI) steel bridge task force and HPS Design Advisory Group, in close cooperation with the AASHTO T-14 committee (Steel Bridges).

The 1998 version of the AASHTO LRFD Bridge Design Specifications marked the first time where design limitations were imposed (AASHTO, 1998). The following is a summary of the various design issues that either had HPS related limitations in the 1998 version of the AASHTO code or were a concern for designers (Azizinamini *et al.*, 2004).

- For continuous plate girders with compact negative sections, the maximum moment capacity was limited to yield moment capacity of the section, M_y, rather than the plastic moment capacity, M_p, as used for lower grade steels.
- Inelastic methods of analysis and design were not permitted for HPS plate girders with yield strength equal to or exceeding 70 ksi. It should be noted that this also disallows the use of the 10% moment redistribution for girders comprised of compact sections.
- Information to check the ductility of composite plate girders in the positive section, per requirements stated in section 6.10.4.2.2 of the AASHTO LRFD Bridge Design Specifications, was incomplete. As a result, one could conclude that HPS could not be used in the positive sections since ductility check provisions were not available.
- In the initial stages of introducing HPS, there was a concern that HPS plates may not be able to sufficiently develop large tensile strains without fracture. Some of the examples included use of HPS as tension flanges of plate girders in positive sections or use of HPS as tension members in trusses. These concerns were mainly a result of work by McDermott (1969) who conducted tests on A514 100 ksi steel girders. When these girders were loaded in three-point bending, the high strength steel tension flange fractured very shortly after yielding.
- For years, AASHTO codes had limited the shear capacity of the hybrid plate girders to the elastic buckling capacity of the panel. Hybrid girders consist of using higher grades of steel for flanges and lower grades for the web. For instance, using 50 ksi steel for flanges

and 36 ksi steel for webs, or using 70 ksi steel for flanges and 50 ksi steels for webs. This limitation was not confined to HPS. It also applied to hybrid girders fabricated with 50 and 36 ksi steels. What made this limitation important was the fact that it has been shown that the best use of HPS in plate girders is in the hybrid form where flanges are constructed using 70 ksi steels and webs are constructed using 50 ksi steels (Horton *et al.*, 2000). Design studies have indicated that for many typical situations, hybrid girders will produce the most economical designs (Barker and Schrage, 2000; Horton *et al.*, 2000; Clingenpeel and Barth, 2003).

- Current specifications place limits on the maximum allowable live load deflections. These requirements have not typically controlled the geometry of sections designed with steel having f_y < 50 ksi. However, due to the reduced section geometries required when HPS 70W steel is incorporated, these limits may be the controlling limit state for some design situations. Therefore, research has been initiated to investigate the rationale behind the current limits and to assess their influence on the serviceability and economy of HPS bridges.
- In addition to incorporating HPS 70W in traditional I girder configurations, it was felt that innovative concepts capitalizing on both the increased strength and improved toughness of the steel may also produce cost effective structures. Some of the design innovations that have been developed may prove to be beneficial for various steel grades (e.g., Grade 50, HPS 70W and HPS 100W, with minimum yield strength of 100 ksi).

1.1.2 Live-load deflections

The AASHTO Standard Specifications (1996) place a limit on the maximum allowable live-load deflection of L / 800 for most bridges and L / 1000 for bridges subject to pedestrian use. Similar specifications are given in the AASHTO LRFD Specifications (1998), which are specifically written as optional criteria; however, many state transportation departments will continue to view them as mandatory requirements (Azizinamini *et al.*, 2004). For traditional steel bridges comprised of steels with f_y < 50 ksi, these limits have rarely been found to control girder geometries. However, recent studies have shown that for some design situations with HPS 70W, particularly in cases with high span-to-depth ratios, these limits may have a significant influence on the final section requirements (Barth *et al.*, 2001; Roeder *et al.*, 2001; Roeder *et al.*, 2004).

A recent research study focusing on examining the influence of these limits on steel I girder bridge design showed that to date there is not a relationship between either reported bridge damage or objectionable vibration characteristics with a direct check of live load deflections (Barth *et al.*, 2001; Roeder *et al.*, 2001; Roeder *et al.*, 2004).

1.1.3 Diagnostic load testing

Field testing is an increasingly important topic in the effort to deal with new infrastructures using new technologies as well as deteriorating infrastructure, in particular bridges and pavements. There is a need for accurate and inexpensive methods for diagnostics, verification of load distribution and determination of the actual load carrying capacity.

Recent studies indicate that over one quarter of the national bridges are either structurally deficient or functionally obsolete, with about half of these involving steel superstructure (FHWA, 2004). The major factors that have contributed to the present situation are ageing,

substantial increase in traffic on existing life-lines, lack of routine inspection and inadequate maintenance in addition to the effect of the harsh and changing environment. The deficient bridges are posted, repaired or replaced, with the disposition of bridges involving clear economical and safety implications. To avoid high costs of replacement or repair, the evaluation must accurately reveal the present load carrying capacity of the structure and predict loads and any further changes in the capacity (deterioration) in the applicable time span (Deza, 2004).

Frequently, diagnostic load tests reveal strength and serviceability characteristics that exceed the predicted codified parameters. Usually, codified parameters are very conservative in predicting lateral load distribution characteristics and the influence of other structural attributes. As a result, the predicted rating factors are typically conservative (Chajes *et al.*, 1997).

1.2 Bridge description

The bridge under investigation (see Figure 1) was recently open to traffic. The bridge is built with five continuous symmetrical spans: the two external are 147 ft and 185 ft long, respectively, while the central one has a length of 200 ft, resulting in a total bridge length of 864 ft. Each internal support consists of reinforced concrete (RC) bents supported by two RC circular piers having a 6 ft diameter. The cross section comprises five composite, equally spaced, HPS I-girders acting compositely with a 8.5 in thick RC deck, with an out-to-out deck and clear roadway width of 40.7 ft and 38 ft, respectively. Cross section and elevation of the girders are provided in Figure 2, while the framing is illustrated in Figure 3.

a) Side view *b) Bridge superstructure under construction*

Figure 1 – Bridge A6358, U.S. Rt. 54/Osage River, Lake of the Ozarks, Miller County, MO

1.3 Objectives

The scope of this project is the assessment of a High Performance Steel (HPS) bridge located at the Lake of the Ozarks in Miller County. The bridge number is A6358 and it is sited on the U.S. Rt. 54/Osage River.

In the project two different innovative techniques for Structural Health Monitoring (SHM) have been applied:

1. An optical non-contact measurement technique, based on an automated target recognition Total Station (TS) system, used to measure the *vertical deflections* of the girders during the pouring of the concrete deck and the diagnostic load test, conducted after the completion of the bridge;
2. A distributed Brillouin sensing technique, utilizing a "smart" glass FRP (GFRP) tape with embedded sensing fibers and bare optical fibers, used to determine the *strain distribution* at different depths of the web for some of the girders. Strains were measured during the diagnostic load test only, since at the time when the deck was poured the optical sensors had not been installed yet.

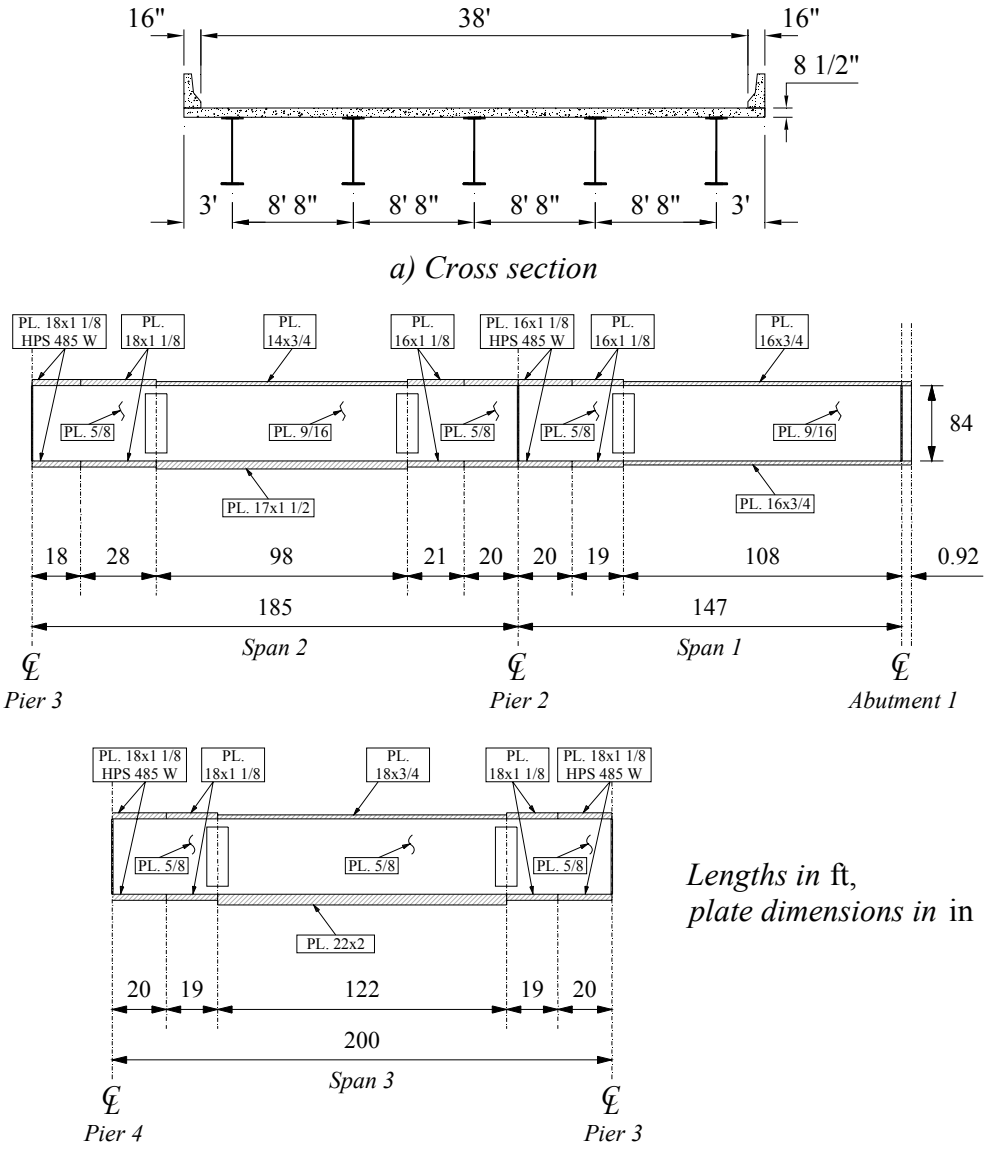

a) Cross section

b) Girder elevation (structural steel ASTM A709 Grade HPS 345 W unless specified)

Figure 2 – Bridge details (not to scale)

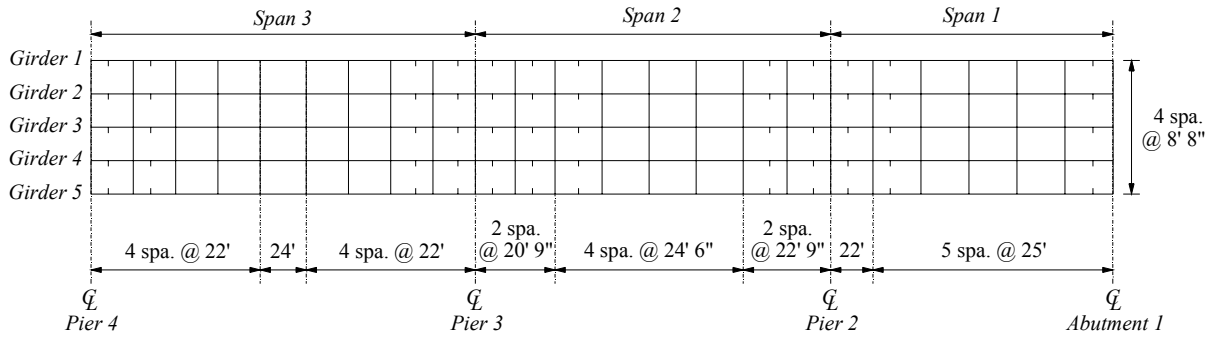

a) Layout

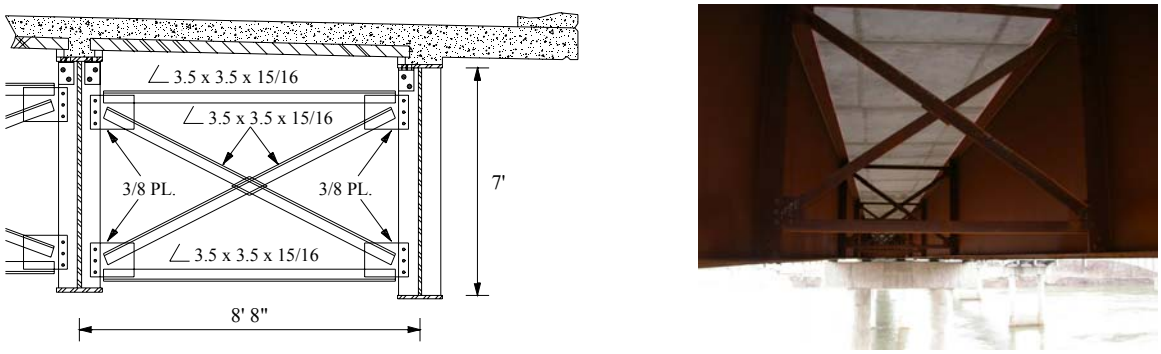

b) Typical cross frame (structural steel ASTM A709 Grade HPS 345 W unless specified)

Figure 3 – Framing plan (not to scale, all dimensions in mm)

1.4 Methodology

To evaluate the response of the bridge, a nondestructive field test was conducted. Experimental load testing on bridges can be either categorized as diagnostic or proof test. In a diagnostic test, a predetermined load, typically near the rated capacity of the structure, is placed at several different locations along the bridge. The corresponding response is measured, and then used to develop a numerical model of the bridge to allow estimating of the maximum allowable load. In a proof test, incremental loads are applied to the bridge until either a target load is reached or a predetermined limit state is exceeded. Using the maximum load achieved, the capacity of the bridge can be determined. Although diagnostic tests provide only an estimate of the load carrying capacity of a bridge, they have several practical advantages including lower cost, shorter testing time, and less disruption to traffic. Because of these advantages, diagnostic testing was used in this case.

The bridge was tested under different static loads using six fully loaded dump trucks, and the comparison between theoretical displacement and strain profiles based on the AASHTO LRFD Bridge Design Specifications (1998) and experimental results allowed determining the safety of the structure.

A major difficulty in the testing and evaluation of bridges in the field is the measurement of vertical deflections. The use of instruments such as mechanical dial gauges, linear potentiometers, linear variable differential transducers (LVDTs), and other similar types of deflection transducers is not always feasible, because a fixed base is needed from which relative

displacements are measured. This often requires access under the bridge to erect a temporary scaffolding to mount the instrument or for running a wire from the instrument to the ground. In the present case, these difficulties were overcome by means of a non-contact deflection measurement technique using an automated target recognition TS system. The solution allows to measure the spatial coordinates of discrete points on a bridge in three dimensions without need of touching the structure. The reliability of this method has been previously demonstrated in a companion report (Galati *et al.*, 2004), where the percentage variation of the total station with respect to LVDTs displacement readings was estimated in the range between 0.1% and 9.7%.

1.5 Description of measurement technologies

1.5.1 Automated Total Station system for deflection measurement

The Automated Total Station (ATS) system used in this project is based on the Leica TCA2003 TS, shown in Figure 4a. The instrument sends a laser ray to reflecting prisms mounted on the structure (Figure 4b) to be monitored. By triangulation with fixed reference points placed outside the structure, the built-in computer can determine the movements of each prism with an accuracy of 0.5" on angular measurements and 0.04 in + 1 ppm on distance measurements, in average weather conditions.

a) Total station

b) Reflecting prism mounted on girder

Figure 4 – ATR TS system equipment for non-contact deflection measurement

TSs have been used to measure the movement of structures and natural processes with good results (Hill and Sippel, 2002; Kuhlmann and Gläser, 2002). Leica Geosystems quotes accuracies of better than 1 mm for their bridge and tunnel surveys. They use a remote system that logs measurements 6 times daily via a modem, with measurements still possible at peak times. Kuhlmann and Gläser (2002) used a reflectorless TS to monitor the long term deformation of bridges. Measurements on a whole bridge were taken every six years and statistical tests were used to confirm whether the points had moved over time. Hill and Sippel (2002) used a TS as part of a multiple-sensor system for landslide monitoring. Merkle (2004) used the TS as part of a 5-year monitoring program for the in-situ load testing prior to and after the strengthening of five existing concrete bridges, geographically spread over three Missouri Department of

Transportation (MoDOT) districts. The five bridges were strengthened using five different Fiber Reinforced Polymer (FRP) technologies as part of a joint MoDOT – University of Missouri-Rolla (UMR) initiative (Lynch, 2004).

There are advantages and disadvantages of using a TS for dynamic deformation monitoring. The advantages include the high accuracy as quoted above, the automatic target recognition which provides precise target pointing (Hill and Sippel, 2002) and the possibility of measuring indoors and in urban canyons in kinematic operating modes (Radovanovic and Teskey, 2001). The disadvantages include the low sampling rate (Radovanovic and Teskey, 2001; Meng, 2002), problems with measurement in adverse weather conditions (Hill and Sippel, 2002) and the need for a clear line of sight between the TS and the prism.

Radovanovic and Teskey (2001) conducted experiments to compare the performance of a robotic TS with GPS. This experiment was conducted because GPS is not an option in many application areas such as indoors. TSs are now capable of automatic target recognition and they can track a prism taking automatic measurements of angles and distances once lock has been established manually. It was found that the TS performed better than GPS in a stop and go situation, where measurements were taken of a moving object only when it was stationary. In a completely kinematic situation, GPS performed the best. It was found that there were two main problems with the TS in kinematic mode; these were a low electronic distance measurement (EDM) accuracy due to a ranging error that was linearly dependent upon the line of sight velocity, and an uneven sampling rate over time worsened by no time tagging.

1.5.2 Brillouin Optical Time-Domain Reflectometry for strain distribution measurement

1.5.2.1 Theoretical foundations

The Brillouin effect is an anelastic scattering process that arises from the interaction between optical and acoustic waves propagating in the same physical medium. The process, sketched in Figure 5, is characterized by a partial energy transfer between the colliding electromagnetic waves (photons) and mechanical wave (phonons). When the medium is illuminated with a monochromatic light source of frequency v_0, there is a spontaneous production of scattered photons characterized by a frequency shift v_a with respect to the incident ones. The shift can be either negative, when the energy hv_a is transferred to the created acoustic phonon, also known as Stokes process, or positive, when it is absorbed from an annihilated acoustic phonon, also known as anti-Stokes process (Brillouin, 1922). Being the energy of the acoustic phonon related to the sound speed in the medium in which the process takes place, the Brillouin wavelength shift is related to the density of the medium, and therefore both with its temperature and mechanical strain. The Stokes process is the most probable due to entropy considerations (Hill *et al*., 1976; Yariv, 1989); it can be observed in silica single-mode optical fibers (Pelous and Vacher, 1975; Thomas *et al.*, 1979).

With the development of novel techniques capable of scanning the Brillouin scattered light spectrum with better resolution, a correlation allowing the evaluation of the strain level from the Brillouin frequency shift was experimentally found (Horiguchi *et al.*, 1989).
Brillouin distributed strain sensing is characterized by a certain number of advantages that make it a very attractive technique for SHM of civil infrastructures.

The main advantage is in the availability of a fully-distributed sensing technique using standard

telecom fiber optics as fully-intrinsic sensors. This results in the following practical considerations:

- The sensor is a standard, inexpensive telecom-grade optical fiber, with easy and immediate off-the-shelf availability for any required length;
- At each point, the fiber acts as a strain sensor, allowing detection and evaluation of phenomena that are hard to locate in advance, such as cracks, debonding, fatigue and defect-triggered faults, along with local discontinuities that cannot be detected on real structures by means of point sensors;
- Low cost, in addition to distributed sensitivity, makes possible long-haul sensors to be installed extensively over the length, area or volume of large structures, thus allowing better understanding of the structural behavior and producing a global overview of the damage distribution, which cannot be retrieved even with long measure-basis sensors;
- Low cost and distributed sensitivity make the system suitable for disposable sensors. For instance, in case of monitoring of tendons during pre-stressing operations, or for emergency sensors that can be left "sleeping" in the structure without heavy additional costs in all cases when it is not possible to know in advance whether the sensor will be used during the life-cycle of the structure or not;
- The whole fiber length can be scanned from the same end point (up to several tenths of km), a characteristic that dramatically simplifies installation and management of cabling;
- Using an Optical Time Domain Reflectometer (OTDR) based on spontaneous Brillouin scattering, no end-to-end full cable continuity is required, which allows operations even with damaged sensing fibers, performing separate scans for the two survival half-lengths.

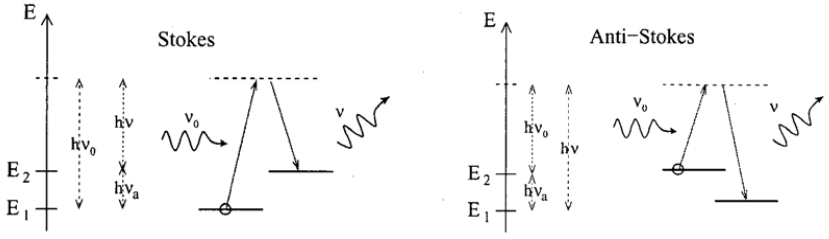

Figure 5 – Representation of quantum energy level of Brillouin scattering process showing both Stokes (left) and anti-Stokes (right) collisions.

In addition to these peculiarities, the Brillouin reflectometry maintains all the advantages that are typical of fiber optic sensing technologies (Casas and Cruz, 2003), *i.e.*

- Absolute insensitivity to Electro-Magnetic Interferences (EMI);
- Long-term durability even in chemically aggressive or harsh environments;
- Current technology top miniaturization grade;
- Complete compatibility with FRP composite materials.

1.5.2.2 Practical applications

Even though primarily developed for telecom cable testing, Brillouin Optical Time-Domain Reflectometry (BOTDR) can be effectively applied for strain distribution monitoring in large-scale civil structures, with some limitations (Komatsu *et al.*, 2002). BOTDR combines the self-heterodyne analysis of the spontaneous Brillouin backscattered light spectrum (Horiguchi *et al.*, 1994), illustrated in Figure 6, with OTDR (Barnoski and Jensen, 1976). The first allows the evaluation of the strain level of a certain length of fiber, while OTDR enables determining the distance along the fiber where the strain information is retrieved by exploiting the relation between the speed of light (c), the sum of the distances traveled by the injected and backscattered light pulses, and the delay time at which the backscattered pulse is detectable (Figure 7).

For the purpose of this test program, the evaluation of the strain distribution has been performed using a Brillouin OTDR AQ8603 optical fiber strain analyzer manufactured by Yokogawa-Ando Corporation of Kawasaki, Japan (Figure 8). The unit allows measurements of strain distribution along a single-mode optical fiber from one end of the optical circuit.

In addition, recent experimental tests have evidenced that performances can overcome the declared limits when the strain distribution under evaluation has no steep discontinuities and has positive peak strain values of at least 100 με. Under these conditions the relative error versus conventional resistive strain gauges has been experimentally shown to be lower than 5% (Bastianini *et al.*, 2003).

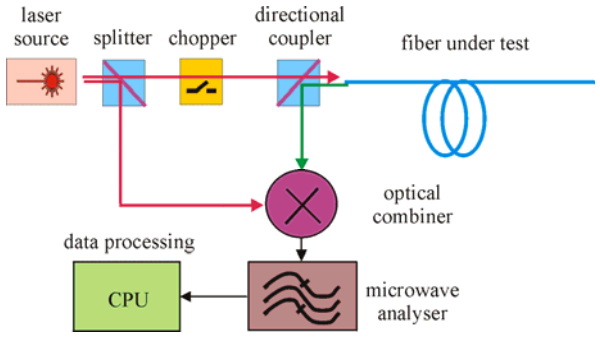

Figure 6 – simplified schematic diagram of self-heterodyne BOTDR.

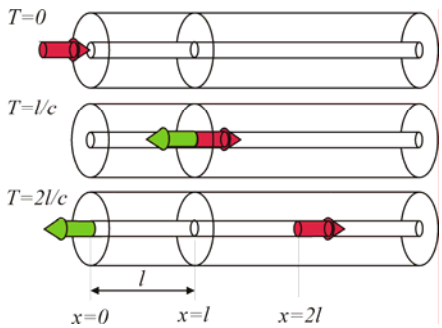

Figure 7 – Schematic of correlation between elapsed time (T) and scanned length (l).

Figure 8 – Brillouin OTDR.

Figure 9 shows the flow chart for structural testing and monitoring using BOTDR technique. It requires the following steps:

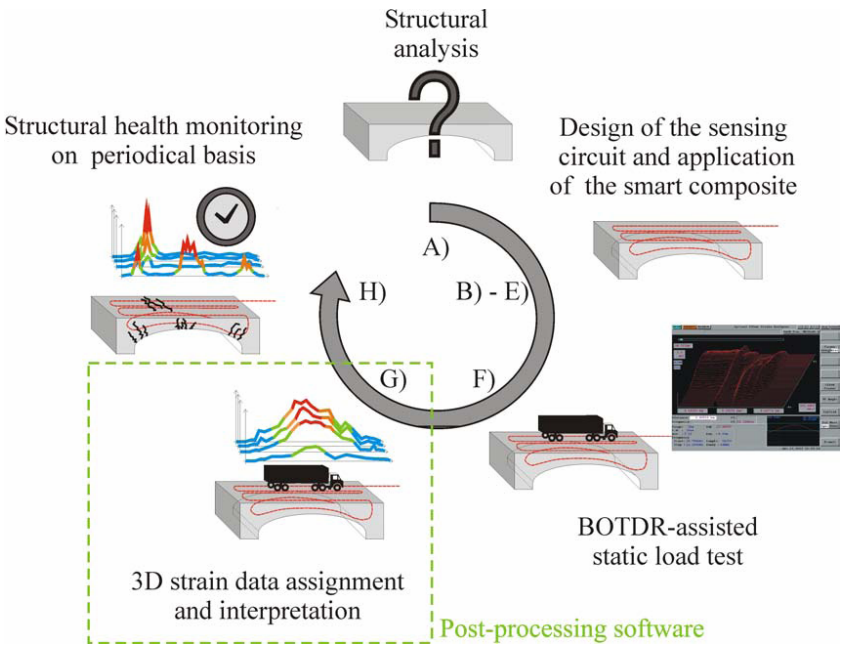

Figure 9 – Brillouin technology for structural monitoring

1. Preliminary structural analysis to identify the areas that have strategic relevance for the structural behavior and are subject to strain value and distributions that are within the detectable strain range of the BOTDR equipment;
2. Design of the optical fiber circuit, including strain sensitive hauls, thermal compensation hauls and access points for future bypass patches in accordance with the areas located during step 1;
3. Installation of the optical fiber circuit providing suitable strain transfer and fiber protection, typically using fiber-equipped "smart" composite materials and other products developed for the specific purpose, and then connecting the various circuit branches through fusion splices and other suitable joints;
4. Optical loss testing in order to ensure that the total optical loss is within the maximum acceptable losses that allow BOTDR operation within the desired accuracy limits;
5. Identification of the 3-D structure points / 1-D sensing fiber correspondence, needed to translate the strain distribution measured along the optical fiber to the strains in the specific areas of the structure equipped with the same fiber. Brillouin co-sensitivity to temperature may be conveniently used in this phase to locate specific temporarily heated points;
6. Load testing of the structure with BOTDR, retrieving the strain distribution along the fiber circuit in different condition, *i.e.* without any load applied and during the various steps of static load tests;

7. Data interpretation, based on the 3-D/1-D correspondence retrieved during step 5;
8. Health status monitoring, performing Brillouin analysis on a periodical basis, or, if required, continuously.

1.5.2.3 Sensing fibers and smart FRP tape

The application of Brillouin fiber optic sensors to a bridge structure introduces a number of problems related to the small order of magnitude of the strains typically achieved during a diagnostic load test, and to the large temperature variations due to prolonged exposure to sunlight. Therefore, it was chosen to use different sensing fibers for strain detection and thermal compensation:

a) 9/125 µm silica single mode fiber with ∅ 900 µm tight PA buffer coating, manufactured by Pirelli Cavi e Sistemi S.p.A., F.ID. 100005827586/FOS_Bast;

b) 9/125 µm silica single mode fiber with ∅ 900 µm loose dry coupled PVC buffer coating, manufactured by Pirelli Cavi e Sistemi S.p.A., F.ID. 100009866510/PIR_Bast;

c) 9/125 µm silica single mode fiber with ∅ 900 µm silicone oil filled PE buffer coating, manufactured by H&S, 01-E9/CW-EW 22600050-110562 F.ID. 1641/2003.

In order to facilitate the installation and reduce the risk of damaging the fibers, an FRP tape with embedded sensing fibers was designed and manufactured. The tape, which is woven from E-glass fiber strands with a 435 g/m^2 warp and a 68 TEX weft, has a width of 100 mm and carries two strain-sensing and two temperature-sensing fibers (Figure 10).

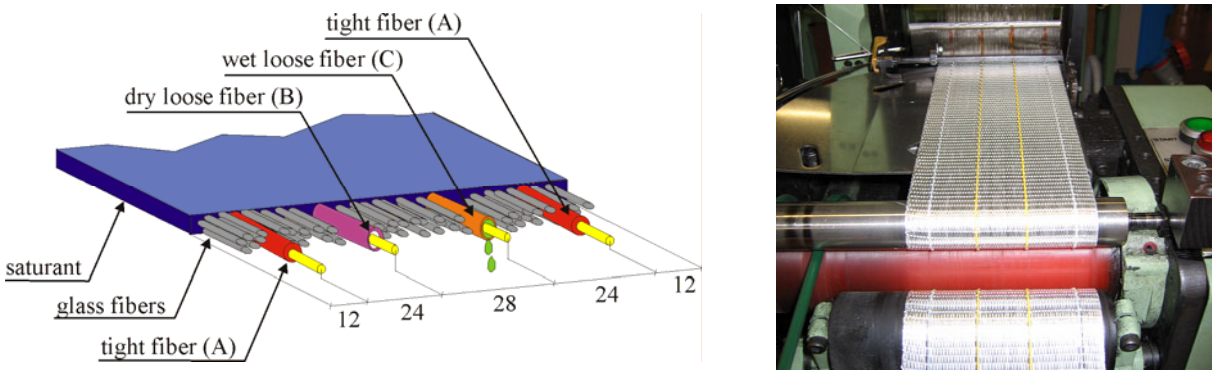

a) Schematic with location of embedded sensing fibers (dimensions in mm)

b) Manufacturing

Figure 10 – Smart GFRP tape

1.5.3 Data Acquisition System

A portable data acquisition unit, custom-manufactured at UMR and suitable for use in field testing of structures (see Figure 11), was used for signal conditioning of the strain gauges installed on the girders to provide a reference data for comparison with the results from BOTDR.

The "Orange Box" is capable of recording 32 high-level channels of data, 16 strain channels, and

32 thermocouple channels, as well as interfacing with TS surveying. The high-level channels may receive DC LVDT's, string transducers, linear potentiometers, or any other +/− 10 Volt DC signal. The strain channels can be used to monitor and record strain gauge signals, load cells, strain-based displacement transducers, or any strain based signal. The 32 thermocouple channels are configured for type T thermocouples.

Figure 11 – Portable data acquisition system ("Orange Box")

The unit consists of a shock-mounted transport box, with removable front and rear covers. Removal of the front cover exposes the computer keyboard and LED display, as well as the front panel of the data acquisition equipment. Removal of the back panel exposes the connector bay, where cables from all the transducers terminate.

The data acquisition system is comprised of National Instruments equipment, listed below:

a) A PXI-1010 SCXI combination unit, which houses the industrial-grade 2.2 GHz Pentium 4 computer, floppy drive, and CDR/W module;

b) A PXI-6030E Analog to Digital converter module for doing the A/D conversion in the system;

c) A pair of SCXI-1520 modules to interface strain based sensors;

d) A SCXI-1102B module for multiplexing high-level sensors;

e) A SCXI-1102B module for multiplexing thermocouple sensors;

f) I/O devices in order to connect additional peripherals and other data acquisition systems such as a Leica TS surveying instrument.

The data acquisition system is controlled by a custom made LabVIEW program installed on a built-in computer, which allows control of data rate, sensor selection and calibration, and display of the data.

2. ATS BASED DISPLACEMENT MEASUREMENT: FIELD EVALUATION

2.1 Bridge instrumentation

A total of 22 prisms were adhesively bonded under the bottom flange along the girders using a cherry picker. Figure 12 depicts the position of the prisms. Targets T1 to T5, T6 to T12 and T13 to T20 along Girder 1, 3 and 5 provided the data to evaluate the longitudinal deformed shape, while the remaining targets were distributed on Girders 2 and 4 to determine the transversal load distribution. Figure 13 shows the reflecting prisms mounted along the first span, between Abutment 1 and Pier 2.

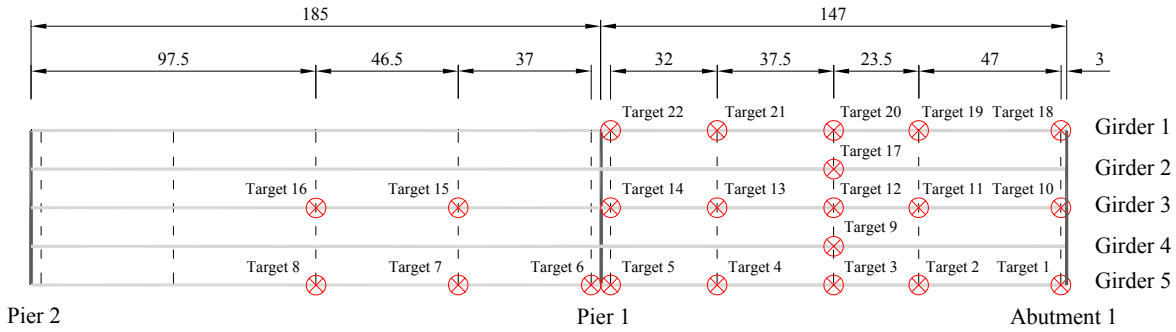

Figure 12 – Target positions: plan view (not to scale, all dimensions in ft)

a) Installation operation *b) Targets in place*

Figure 13 – Reflecting prisms mounted on steel I-girders

An additional prism was mounted on Pier 2 in order to evaluate possible settlements. Finally, two additional prisms were mounted on two piers of the existing bridge running parallel to the one under investigation (Figure 1), and two more prisms were mounted on tripods fixed to the ground. These four additional targets were used as reference points for triangulation.

2.2 Deck installation

2.2.1 Test procedure

Prior to the final load test, the ATS system was utilized to measure the deflections induced by the pouring of the concrete deck (Figure 14). Data were recorded after pouring of progressive deck portions, starting with the first span on the opposite side of Span 1 and 2, where the targets were mounted. The steps are sketched in Figure 15.

a) Casting of concrete *b) Total station running*

Figure 14 – Pouring of concrete deck and deflection measurement *via* ATS

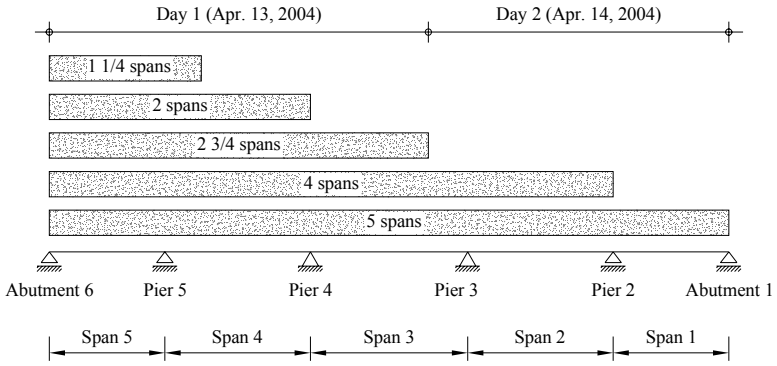

Figure 15 – Progression of deck pouring at deflection measurement steps

Data were retrieved without any interruption of the pouring or interference with the personnel on the bridge. Therefore, the accuracy of the measurements was expected to be influenced also by potential settlements and loading due to the crane and equipment moving along the bridge. In addition, it is envisaged that the deflections during the second day were slightly affected by a certain amount of deck/girder composite action in Span 3, 4 and 5.

2.2.2 Test results

The longitudinal deflections measured during pouring of the concrete deck are summarized in

Figure 16, Figure 17 and Figure 18 for Girder 1, Girder 3 and Girder 5, respectively. Figure 19 shows the transversal midspan deflections in Span 1 measured on Girder 1 to 5 through Target 20, 17, 12, 9 and 3, respectively, wherein data from the same reading have been piecewise connected with straight lines for clarity. Raw data are provided in Appendix II.a.

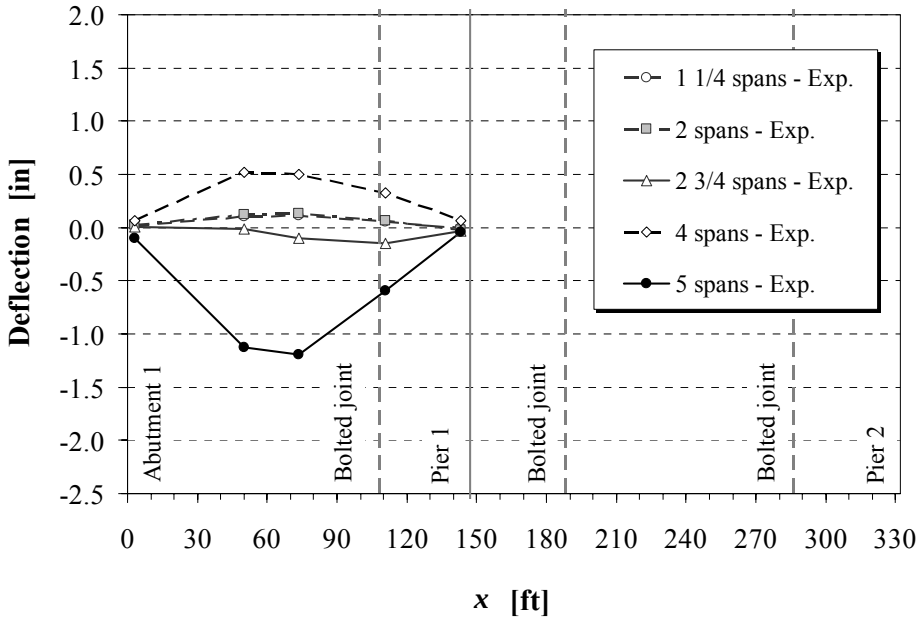

Figure 16 – Measured longitudinal deflections (deck pouring, Girder 1)

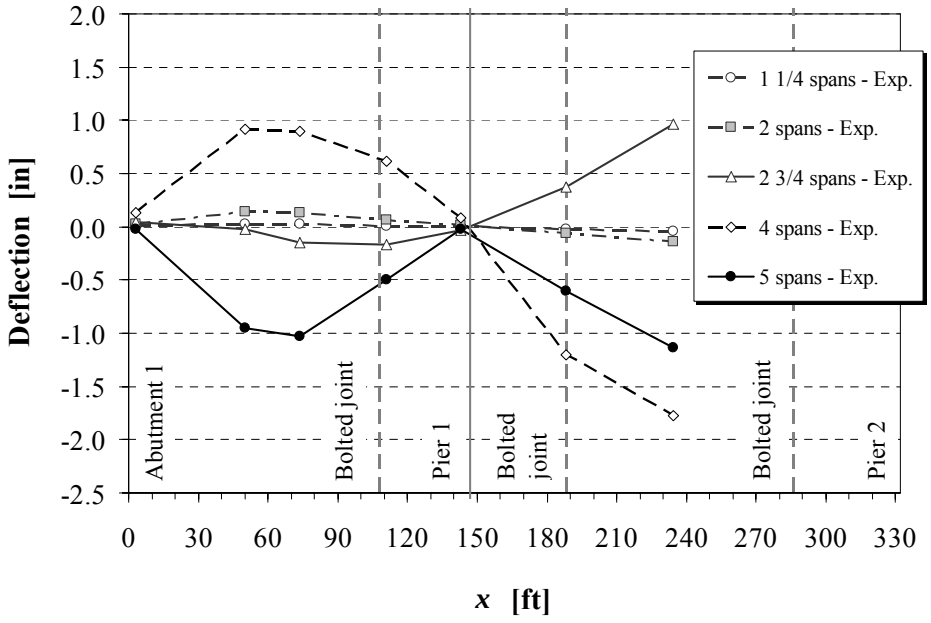

Figure 17 – Measured longitudinal deflections (deck pouring, Girder 3)

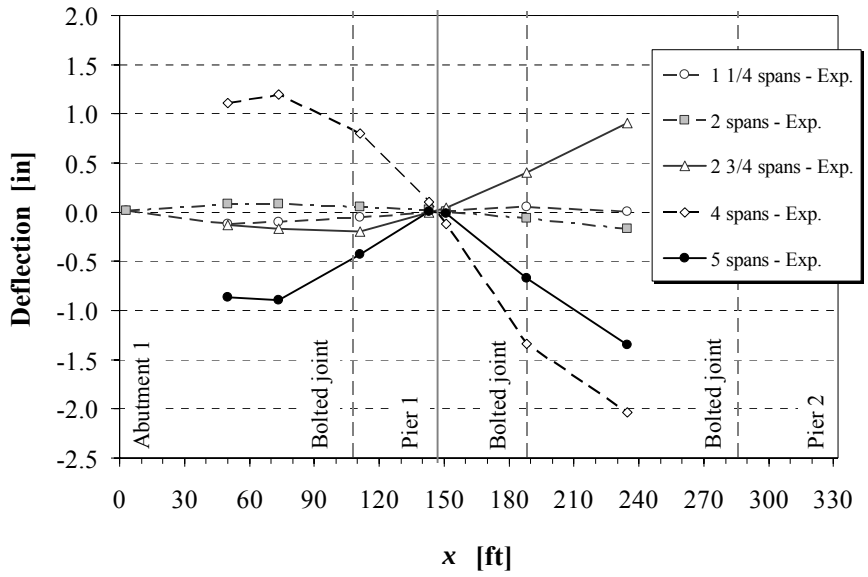

Figure 18 – Measured longitudinal deflections (deck pouring, Girder 5)

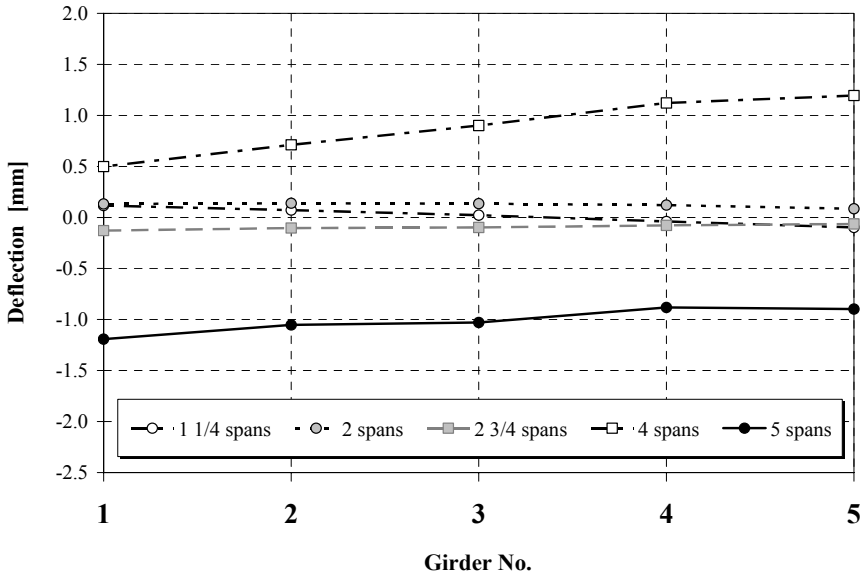

Figure 19 – Measured transversal deflections (deck pouring)

2.2.3 Discussion of results

The experimental deflections were compared with predictions based on 1-D beam analysis. The vertical load per girder was estimated using a tributary area approach and assuming an average thickness of 5.5 in for the concrete layer poured, increased by 3 in along the 3 ft wide overhangs. The actual geometry of each steel girder section was accounted for, as referred to Figure 2b and Table 2.1.

Table 2.1 – Properties of steel girder sections (as in Figure 2b) for deflection computation during deck pouring

Length Interval ***(ft)*** **(Span)**	**Moment of Inertia, I_s** (in^4)	**Flexural Stiffness, E_sI_s (E_s = 29 msi)** $(kip \cdot in^2)$
0-108 (1)	70,879	2.06E+09
108-188 (1,2)	96,090	2.79E+09
188-286 (2)	88,245	2.56E+09
286-371 (2,3)	104,243	3.02E+09
371-432 (C.L., 3)	108,323	3.14E+09

Figure 20, Figure 21 and Figure 22 show the comparison between analytical and representative experimental results for Girder 1, 3 and 5. It can be observed that the predictions fairly describe the measured deflections. Some apparent inconsistencies due to relatively high deflections for Girders 1, 3 and 5, as the concrete was poured on Span 4 in particular, and Span 5, may be attributed to the following variables:

- Additional loading due to the steel crane, loading the two external girders directly, and the workers and equipment moving along the bridge during the pouring operations (see Figure 14);
- Deflections induced by thermal loads;
- Settlements, due to the additional uniform dead load of the concrete poured;
- Deck/girder composite behavior in Span 3, 4 and 5, as far as the measurement of the second day are concerned, as the concrete poured during the first day was already considerably hardened;
- Approximation of the loading steps considered in the calculations (see Figure 15) versus the actual load conditions, as the pouring operations were never interrupted for deflection measurement purposes, in order not to interfere with the personnel on the bridge.

However, it is noted that a comparison between Figure 20d and Figure 22d points out a rather significant midspan deflection of Girder 1 (1.193 in), which is 32% and 14% greater than the correspondent in Girder 5 (0.898 in) and the theoretical value (1.025 in), respectively. Due to the variety of factors that may affect measurements, as specified above, more thoughtful conclusions cannot be drawn herein.

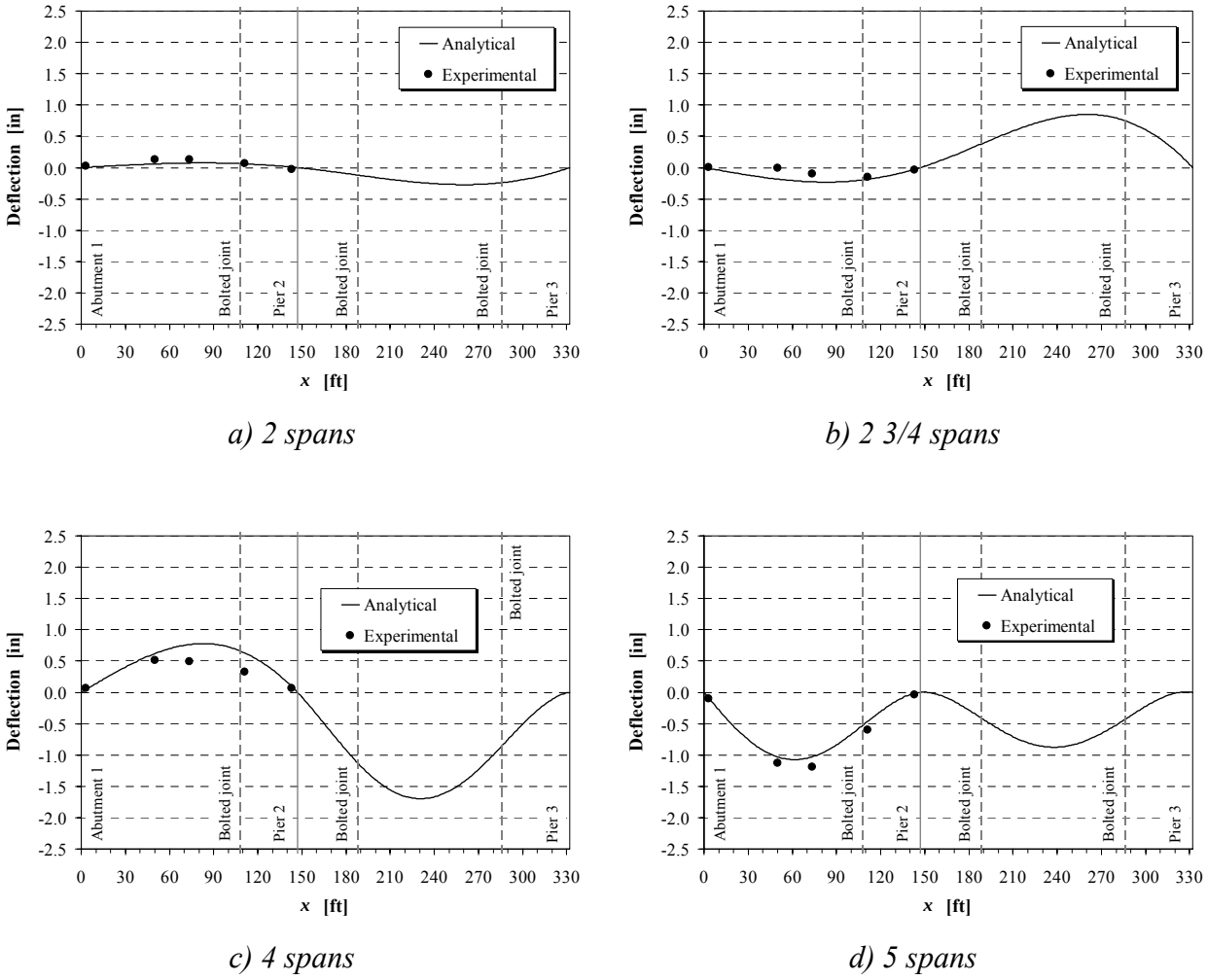

Figure 20 – Comparison between theoretical and experimental longitudinal deflections (deck pouring, Girder 1)

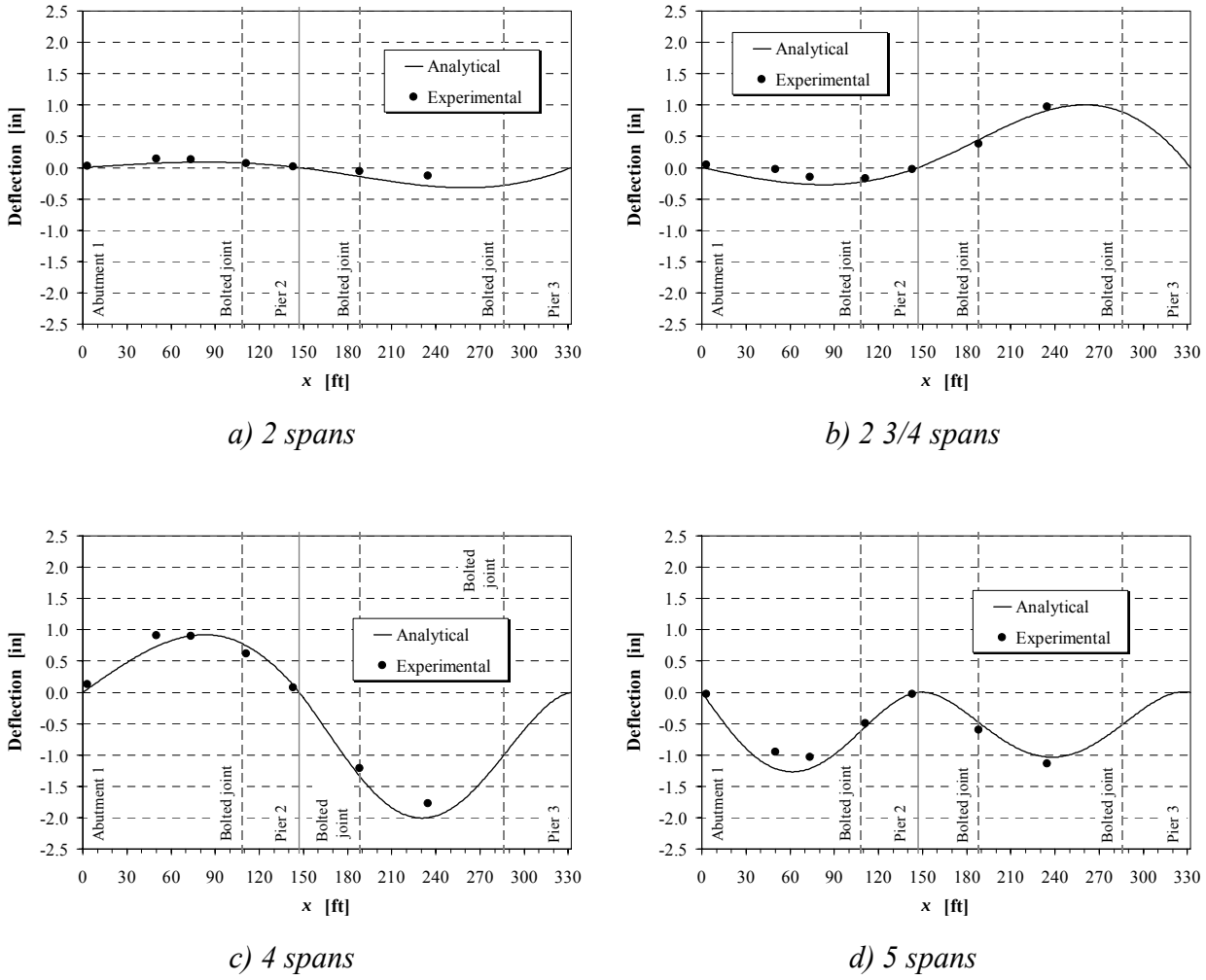

Figure 21 – Comparison between theoretical and experimental longitudinal deflections (deck pouring, Girder 3)

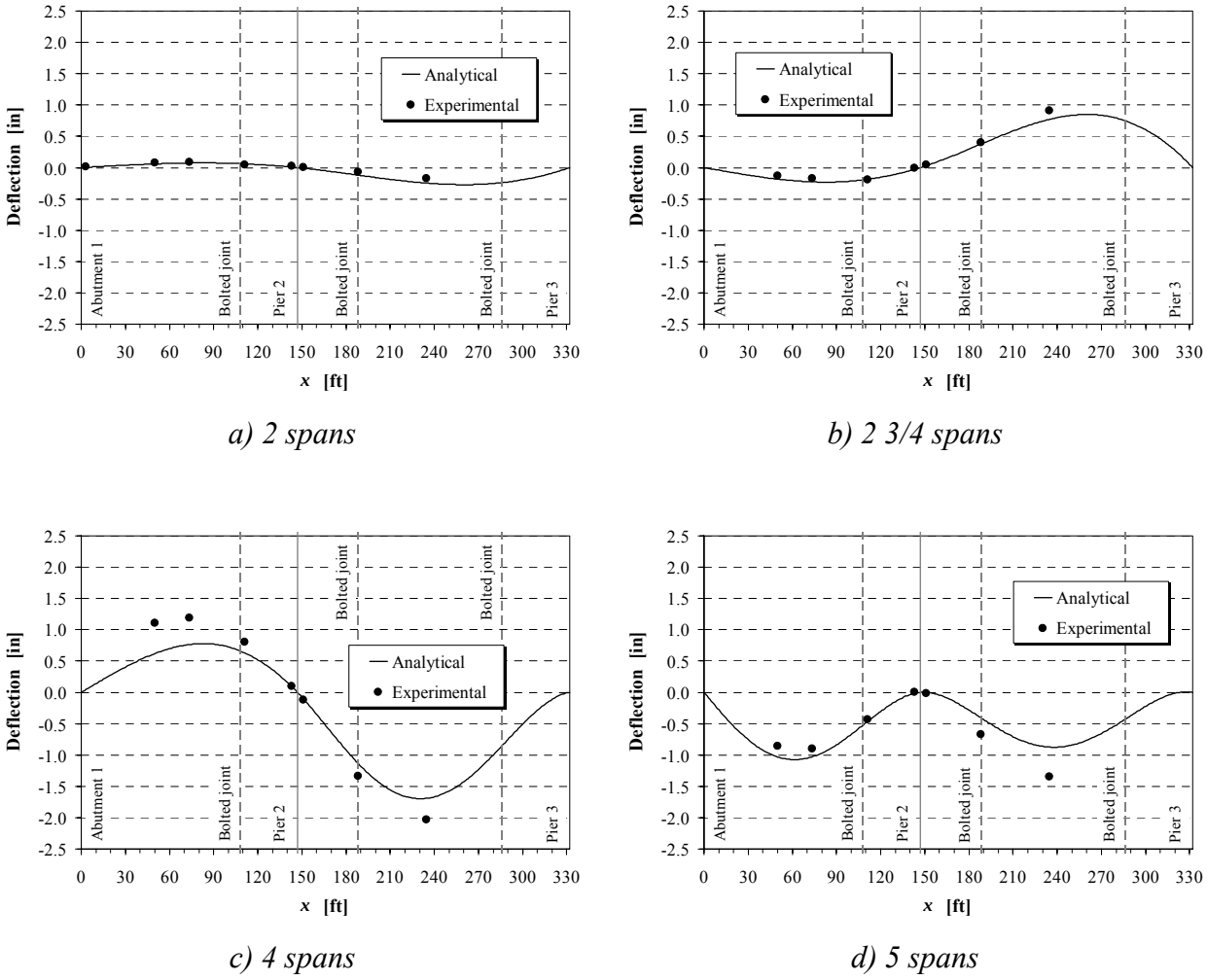

a) 2 spans

b) 2 3/4 spans

c) 4 spans

d) 5 spans

Figure 22 – Comparison between theoretical and experimental longitudinal deflections (deck pouring, Girder 5)

2.3 Load test

2.3.1 Test procedure

The load test was carried out using six fully loaded 10-wheel three-axle dump trucks. Axles spacing and width are shown in Figure 23.

(a) Trucks on site

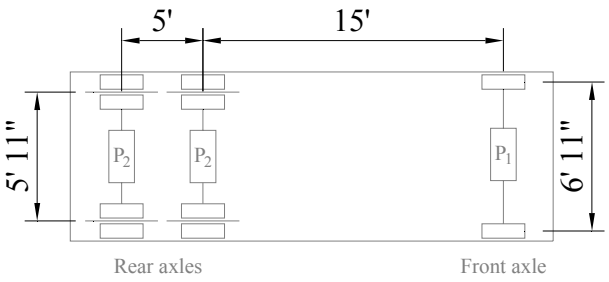

(b) Spacing and width of axles

Figure 23 – Dump trucks used for load test

The trucks were weighed before testing and coded with a number from 1 to 6. Table 2.2 summarizes weight and assumed load distribution between front and rear axles.

Table 2.2 – Dump trucks used for load test: weight distribution assumed for analysis

Truck No.	**Total Weight** *(kips)*	**Front Axle (P_1)** *(kips)*	**Each Rear Axle (P_2)** *(kips)*
1	45.4	17.0	14.2
2	43.3	16.2	13.5
3	53.1	19.9	16.6
4	54.8	20.6	17.1
5	60.2	22.6	18.8
6	56.4	21.2	17.6

A total of eight stops were planned, and details are reported in Appendix I. Marks were made on the concrete deck to indicate the trucks stops, and the distance between the front axle of each truck and the rear axle of the truck in front in the line load was 9 ft.

Stop 1, 2 and 7 were intended to produce the maximum deflections on Girder 1 and 5 using both directions of traffic with two symmetrical lanes of two (Stop 1) and three (Stop 2 and 7) trucks each. Stop 3, 4 and 6 were intended to produce the maximum deflections on Girder 5 in Span 3,

2 and 1, respectively, using a train of six trucks. Stop 5 was planned to induce the maximum negative moment on Girder 5, at Pier 2. Finally, Stop 8 was intended to produce the maximum deflections on Girder 1 in Span 1 using a single lane of six trucks. Figure 24 shows the transverse position of the trucks for the different stops.

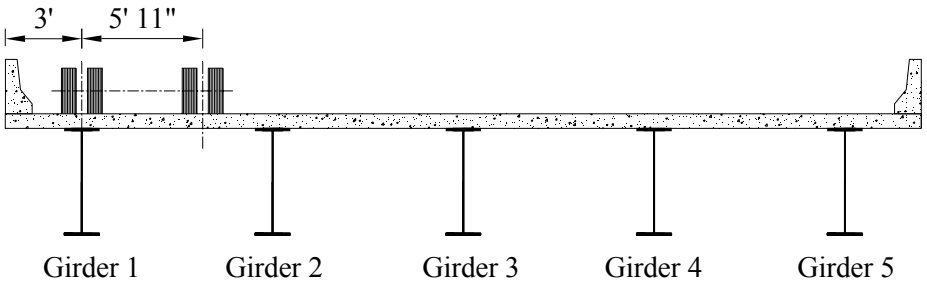

(a) Stop 8

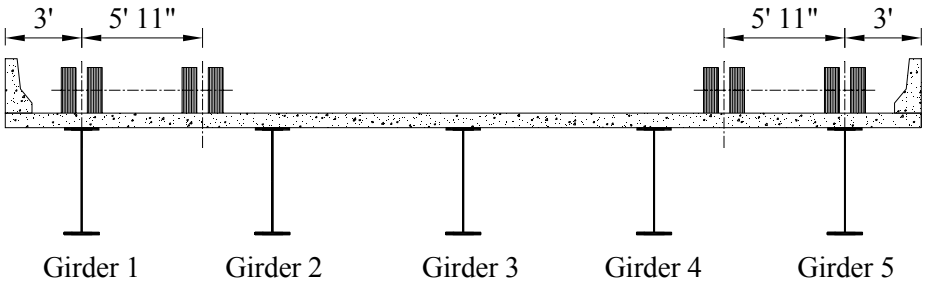

(b) Stop 1, 2 and 7

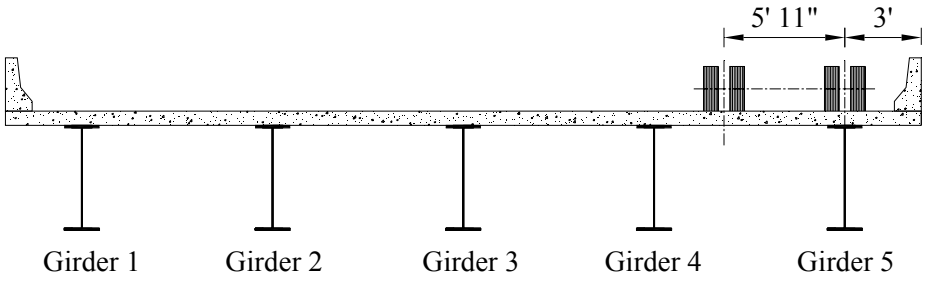

(c) Stop 3, 4, 5 and 6

Figure 24 – Transverse position of trucks during load test (not to scale)

In order to minimize the influence of systematic errors in the displacement measurements, and during the load test only, the TS was mounted on a leveling steel plate fixed on a concrete pile (Figure 25).

Once the TS was leveled and acclimatized, initial readings were taken for each prism. Then, the trucks drove to the first stop. At each stop, 15 minutes were allowed for potential settlements, before acquiring the data. To ensure stable measurements, four readings were taken for each target, two direct and two inverse, in order to average out possible errors. Once the reading was terminated, the trucks moved to the next stop and the same procedure was repeated.

Figure 25 – Total station in load test configuration

2.3.2 Test results

Figure 26, Figure 27 and Figure 28 show the longitudinal deflections of Girder 1, Girder 3 and Girder 5, respectively, corresponding to all the eight stops during the load test, while Figure 29 summarizes the transversal distribution of deflections at the mid-span between Abutment 1 and Pier 2. Data from the same stop have been piecewise connected with straight lines for clarity. Raw data are provided in Appendix II.a.

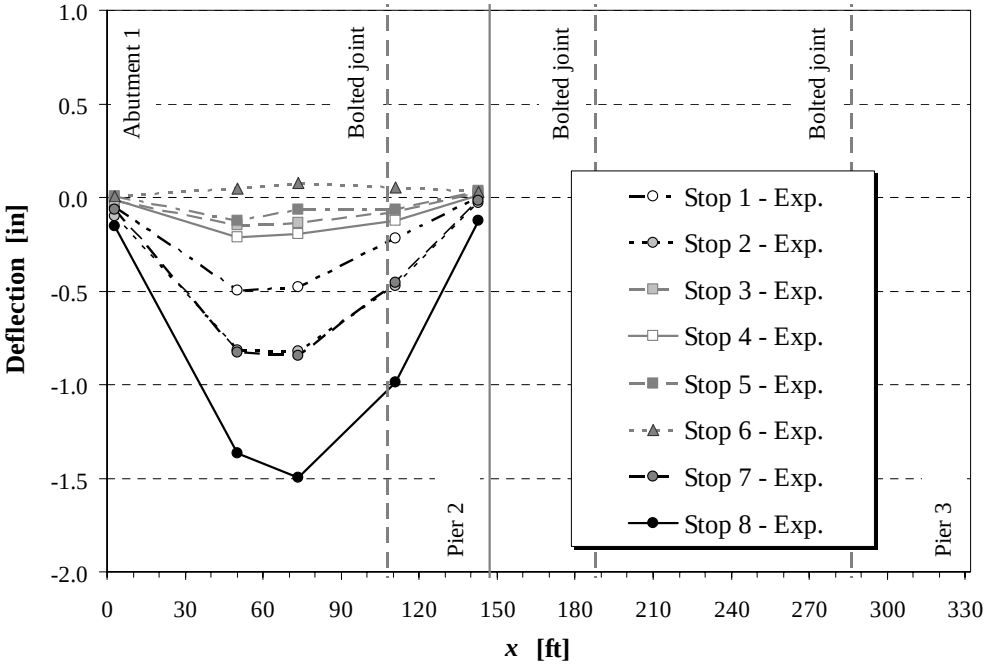

Figure 26 – Experimental longitudinal deflection (load test, Girder 1)

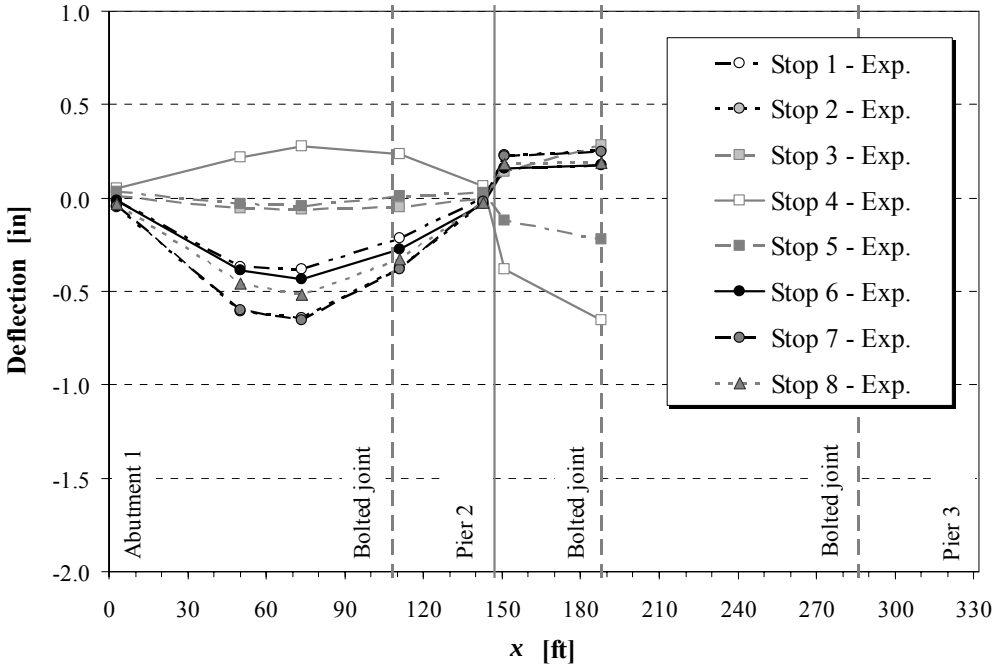

Figure 27 – Experimental longitudinal deflections (load test, Girder 3)

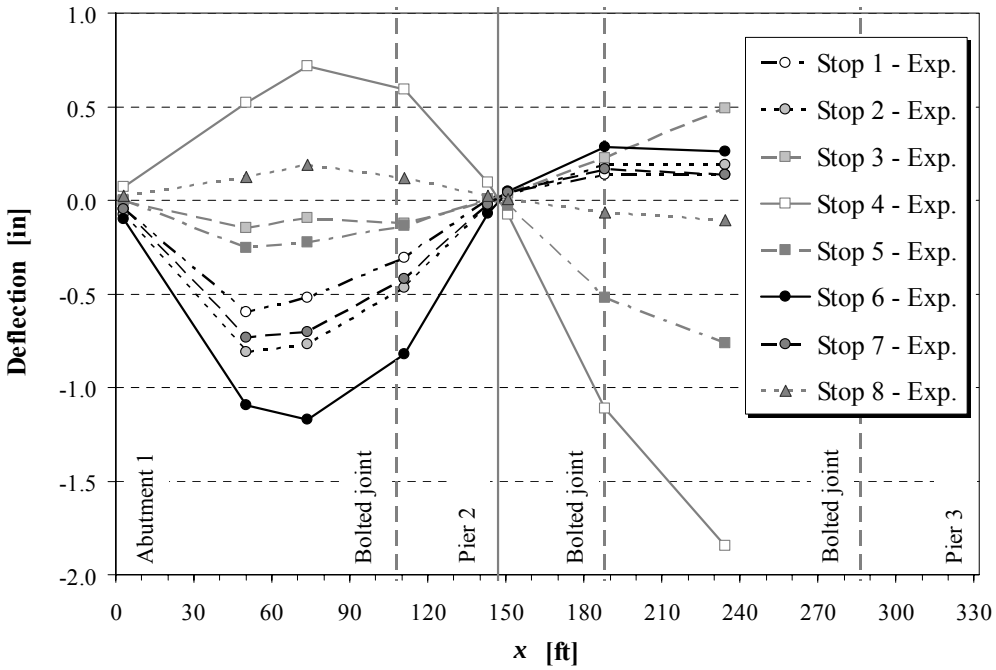

Figure 28 – Experimental longitudinal deflections (load test, Girder 5)

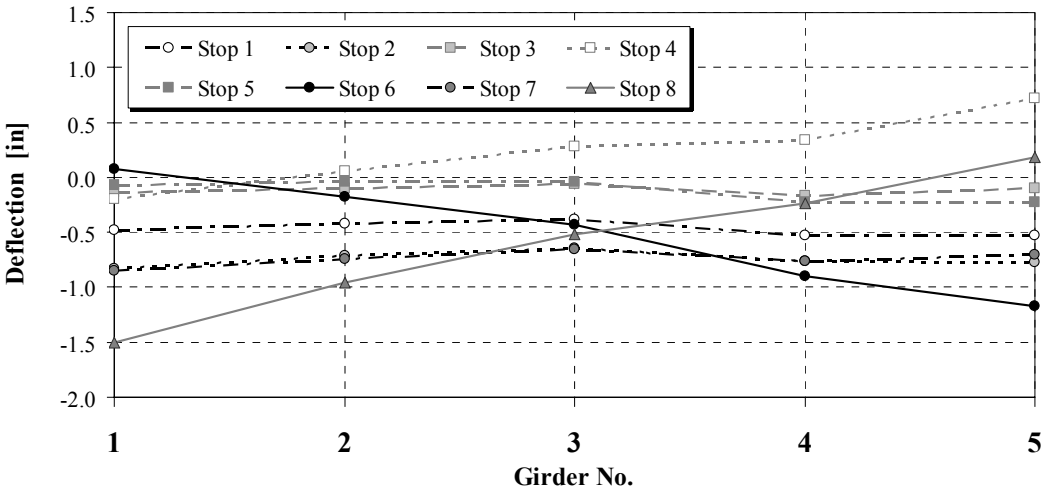

Figure 29 – Experimental transversal deflections at midspan of Span 1 (load test)

It can be observed that the readings are consistent from stop to stop, while the curves generally exhibit a smooth transition from point to point. However, a comparison between the deflections of Girder 1 and 5 during Stop 8 and 6, points out that the first reached values 28% higher when subjected to absolutely similar load conditions, as shown in Figure 30. Such difference cannot be explained by accounting for possible concurrent factors that played a role in determining the measurement results. A preliminary, yet reasonable explanation may lie in the fact that Girder 1 fell during construction (Figure 30), due to the action of wind, and likely experienced some damage either during the falling or re-positioning. This calls for further verification by means of the results from BOTDR based strain measurement, along with a comparison with analytical and numerical predictions.

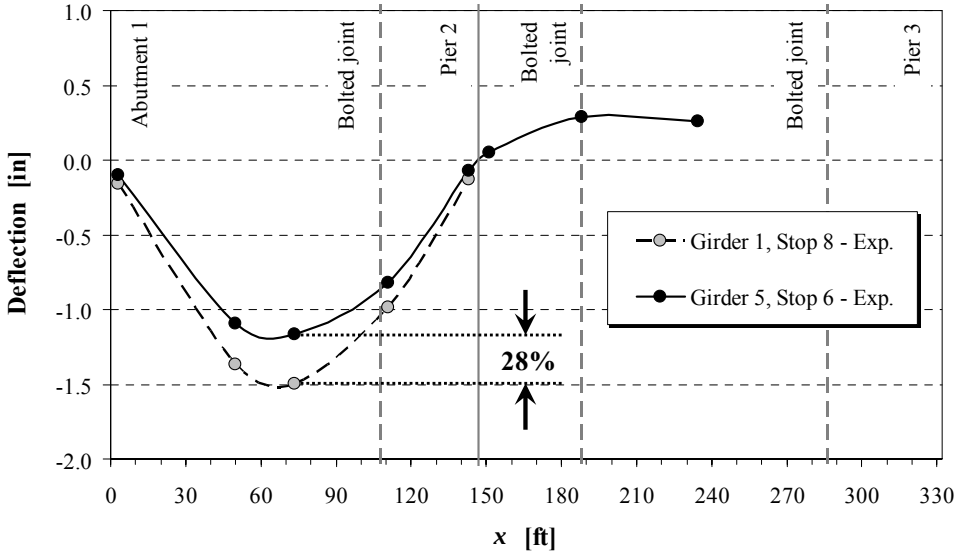

Figure 30 – Experimental deflections for Girder 1, Stop 8 and Girder 5, Stop 6 (load test)

Figure 31 – Girder 1 fallen due to wind during erection of bridge superstructure

2.3.3 Discussion of results

The experimental deflections of Girder 1, 2, 4 and 5 were compared with results based on 1-D beam analysis. The girder distribution factors, GDF (defined as the ratio of the maximum moment on a girder at a given live load condition, and the maximum theoretical moment determined by applying the entire load truck to a single composite girder), were determined according to the AASHTO Bridge Design Specifications (1998), [Table 4.6.2.2.2d-1]. A multiple presence factor m = 1 was assumed when using the lever rule. Adjustments in the negative moment region near the interior support (Pier 2) due to continuity effects have been neglected. Details of calculations are summarized in Table 2.3 and Table 2.4.

Table 2.3 – GDFs as per AASHTO LRFD Bridge Design Specifications (1998)

Girder No.	No. of Lanes Loaded	AASHTO Formula	GDF Span 1	GDF Span 2
1, 5	1	Lever rule	0.658	0.658
2, 4	1	$\text{GDF} = 0.06 + \left(\frac{S}{168}\right)^{0.4}\left(\frac{S}{L}\right)^{0.3}\left(\frac{K_g}{Lt_c^3}\right)^{0.1}$	0.432[a]	0.406[a]
1, 5	2[c]	$\text{GDF} = e \cdot \text{GDF}_{2,4},\ e = 0.77 + \frac{d_e}{109.2} \geq 1$	0.641[a,b]	0.613[a,b]
2, 4	2[c]	$\text{GDF} = 0.075 + \left(\frac{S}{114}\right)^{0.6}\left(\frac{S}{L}\right)^{0.2}\left(\frac{K_g}{Lt_c^3}\right)^{0.1}$	0.641[a]	0.613[a]

[a] See Table 2.4 for parameters and units

[b] d_e = distance from center of exterior beam and inside edge of barrier = 36 – 16 = 20 in, therefore e = 1

[c] In the case of two load lanes (Figure 24b), the closer to the girder considered was assumed for computation

Table 2.4 – Input data for calculation of GDFs (AASHTO, 1998)

Parameter	(unit)	Definition	Value (Span 1)	Value (Span 2)
S	(in)	Girder spacing	104	104
L	(in)	Span length	1,764	2,220
K_g	(in^4)	Longitudinal stiffness parameter $= \frac{E_s}{E_c}\left(I_s + A_s e_g^2\right)$	$1.836 \cdot 10^6$	$2.189 \cdot 10^6$
E_s	(ksi)	Modulus of elasticity of steel (girder)	29,000	29,000
E_c	(ksi)	Modulus of elasticity of concrete (deck)	3,605	3,605
I_s	(in^4)	Moment of inertia of steel girder section	70,879	88,245
A_s	(in^2)	Area of steel girder section	71.25	83.25
e_g	(in)	Distance between center of gravity of girder section and concrete deck	47.0	47.0
t_c	(in)	Thickness of concrete deck	8.5	8.5

The width of the concrete slab section was selected as the average spacing of adjacent beams [4.6.2.6.1], *i.e.* S = 104 in, for both interior and exterior beams. It is noted that the contribution of the structurally continuous concrete barrier has been accounted for [C4.6.2.6.1-1], thus determining a theoretical flange width for the external girder as

$$\frac{S}{2} + w_{overhang} + \frac{A_b}{2t_c} \simeq \frac{104}{2} + 36 + \frac{328}{2 \cdot 8.5} \simeq 107.3 \text{ in},$$

wherein $w_{overhang}$ is the width of the overhang (in), A_b the cross sectional area of the barrier (in^2), and t_c the deck thickness (in). Since the difference between the flexural stiffness of the equivalent interior and exterior girders is of the order of 0.5%, the 104 in flange width was used for all the beams.

Figure 32 and Figure 33 show the comparison between the deflections measured on Girder 1 and 5, respectively, and the analytical deformed shapes. The deflections measured through the ATS system are generally smaller than the theoretical values, and clearly well below the L / 800 limit [2.5.2.6.2] of 2.2 in and 2.8 in on Span 1 and Span 2, respectively, as shown in Figure 32d and Figure 33d and f, thereby demonstrating the safety of the structure. Nevertheless, comparison of Figure 32d and Figure 33d and f points out the tendency of Girder 1 to approach the theoretical limits, differently from Girder 5, when directly subjected to essentially the same load conditions. As previously mentioned, the falling of the girder occurred during construction may have determined some alteration of the structural response, which may call for further assessment.

Conversely, the response of Girder 5 confirms the conservativeness of the design provisions.

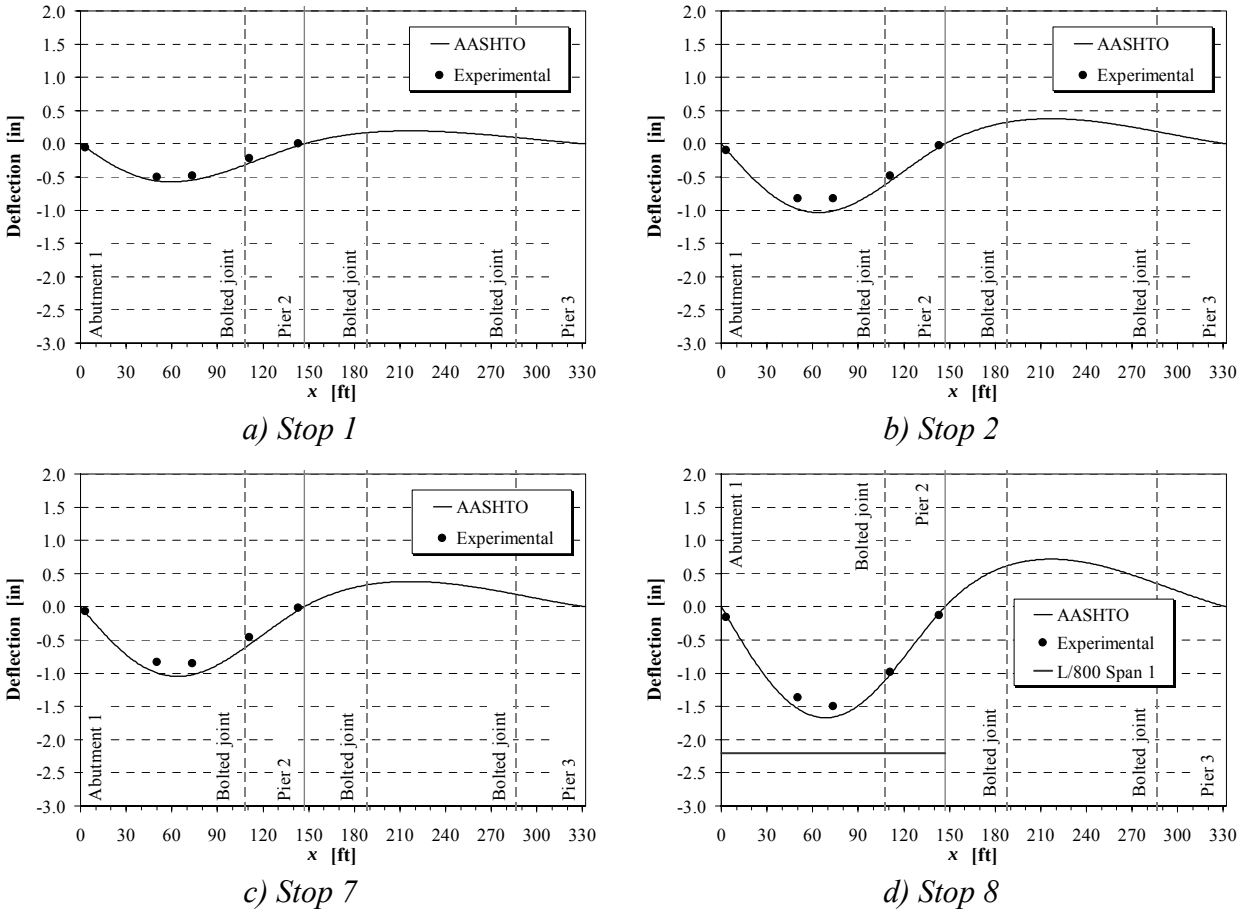

Figure 32 – Comparison between AASHTO provisions and experimental longitudinal deflections (load test, Girder 1)

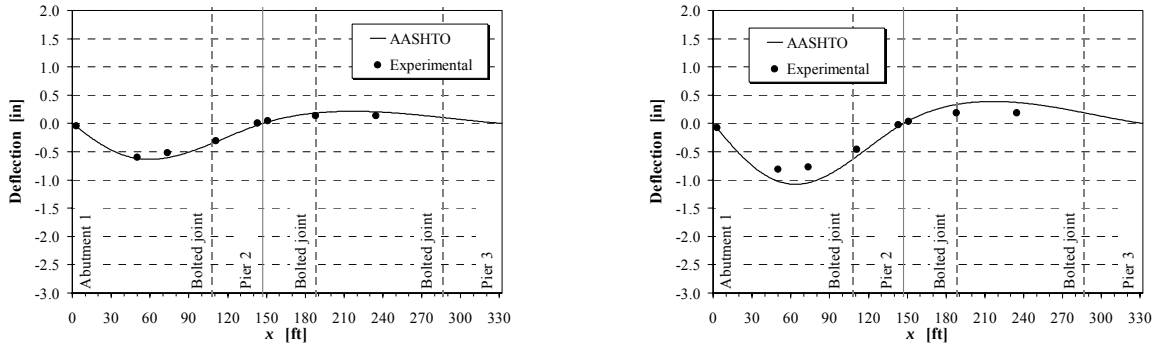

a) Stop 1

b) Stop 2

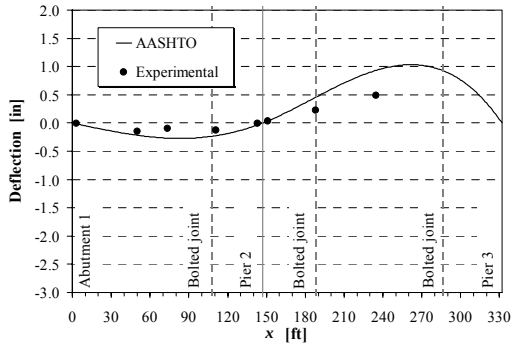

c) Stop 3

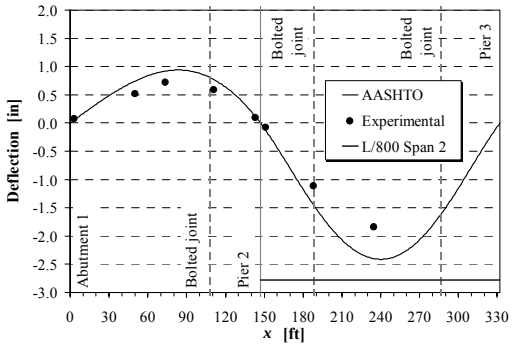

d) Stop 4

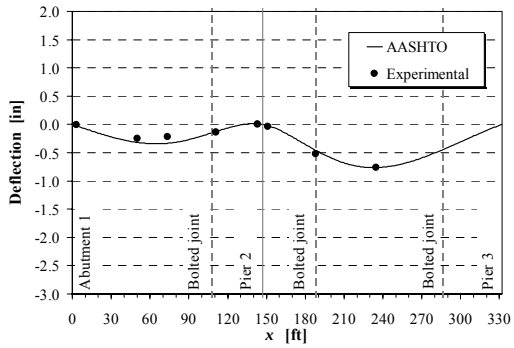

e) Stop 5

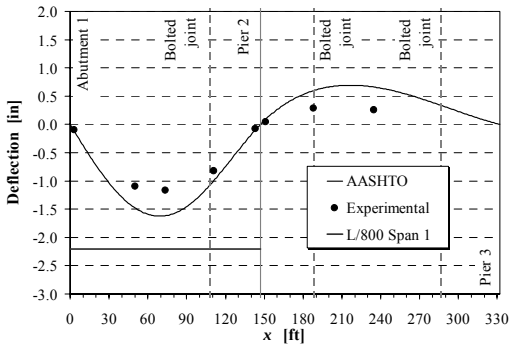

f) Stop 6

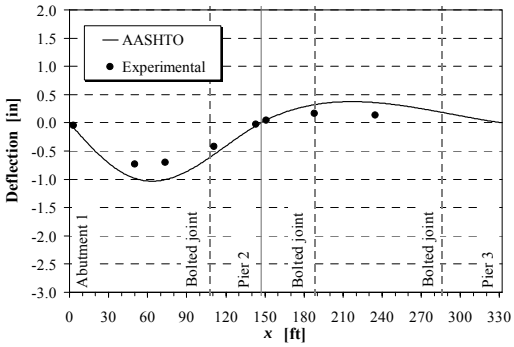

g) Stop 7

Figure 33 – Comparison between AASHTO provisions and experimental longitudinal deflections (load test, Girder 5)

Since all the beams considered for the 1-D analysis were assumed to have essentially the same geometrical and material characteristics, *i.e.* an equivalent flexural stiffness, the GDF for the *i*th girder at the midspan in Span 1 was estimated from the deflection data retrieved as

$$\mathrm{GDF}_i = \delta_i / \sum_{j=1}^{5} \delta_j,$$

wherein δ_i = deflection of the *i*th girder. Figure 34 and Figure 35 show the distribution factors calculated at each stop with one and two lanes loaded, respectively.

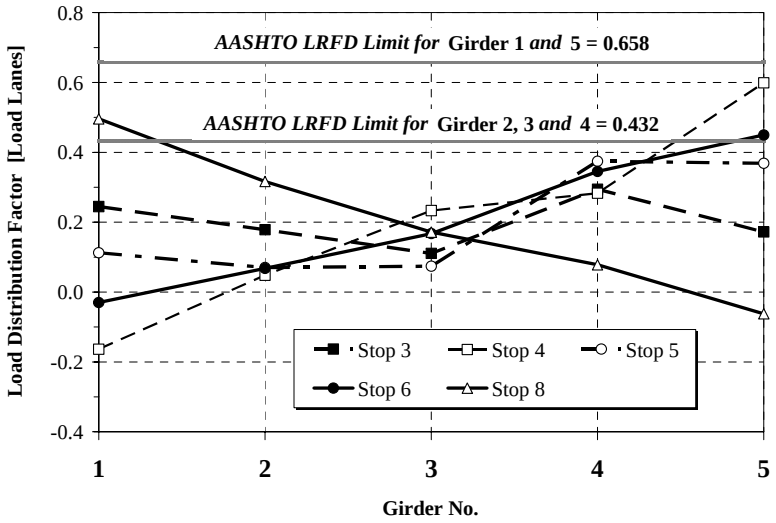

Figure 34 – Comparison between AASHTO and experimental girder load distribution factor at midspan between Abutment 1 and Pier 2 in case of one lane loaded (Stop 3, 4, 5, 6 and 8)

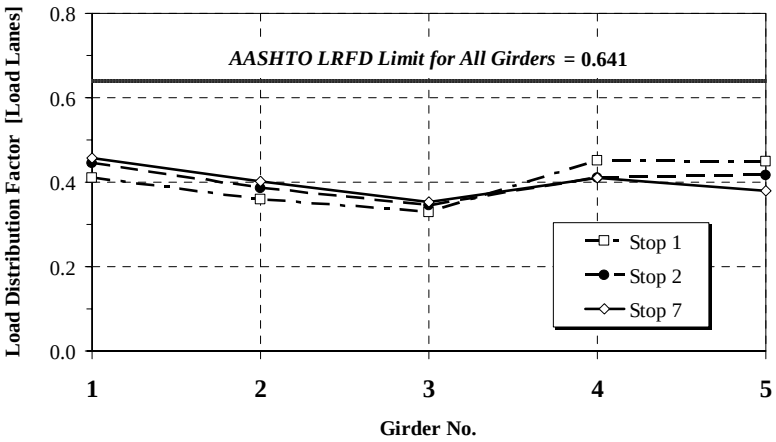

Figure 35 – Comparison between AASHTO and experimental girder load distribution factor at midspan between Abutment 1 and Pier 2 in case of two lanes loaded (Stop 1, 2 and 7)

midspan between Abutment 1 and Pier 2 in case of two lanes loaded (Stop 1, 2 and 7)

The load distribution factors determined experimentally at the midspan section between Abutment 1 and Pier 2 (Figure 12) are always smaller than those based on the AASHTO provisions, which are proved to be conservative for the case under consideration. The main reason typically lies in the inherent conservativeness of neglecting the transverse stiffening action of the diaphragms when using either the design formulas, wherein the thickness of the deck is the only parameter that explicitly accounts for a degree of transverse stiffness in the structural system, or the lever rule.

3. BOTDR BASED STRAIN MEASUREMENT: FIELD EVALUATION

3.1 Bridge instrumentation

3.1.1 Installation of optical fibers

The sensing elements were installed on Girder 1, 2, 4 and 5. Both the bare optical fibers and the FRP tape with embedded sensing fibers were adhesively bonded onto the girder webs using a two-part epoxy encapsulation resin, after manual surface roughening with steel brushes and degreasing with lacquer thinner. Table 3.1 summarizes the properties of the resin, as provided by the manufacturer (Wabo, 2004). Detailed location and characteristics of the fibers are summarized in Figure 36, Figure 37 and Table 3.2.

Table 3.1 – Properties of Wabo MBrace saturant for fiber optics installation (Wabo, 2004)

Property (Unit)	**Value**
Tensile strength (psi)	8,000
Tensile strain (%)	3.5
Tensile modulus (ksi)	440
Poisson's ratio	0.4
Compressive strength (psi)	12,500
Compressive strain (%)	5
Compressive modulus (ksi)	380
Coefficient of thermal expansion ($^oF^{-1}$)	$20 \cdot 10^{-6}$
Glass transition temperature (^oF)	163

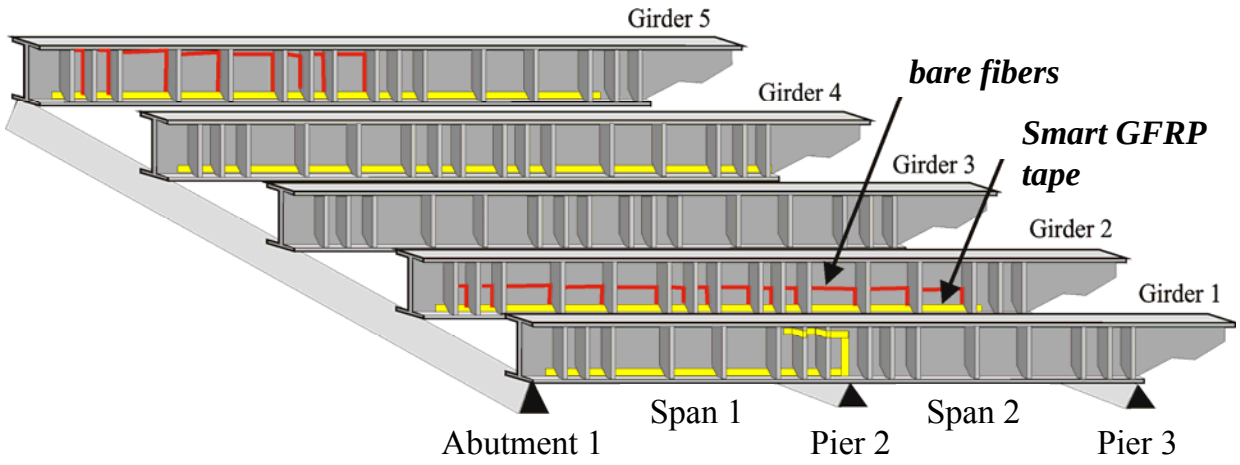

Figure 36 – Schematic of fiber circuit placement

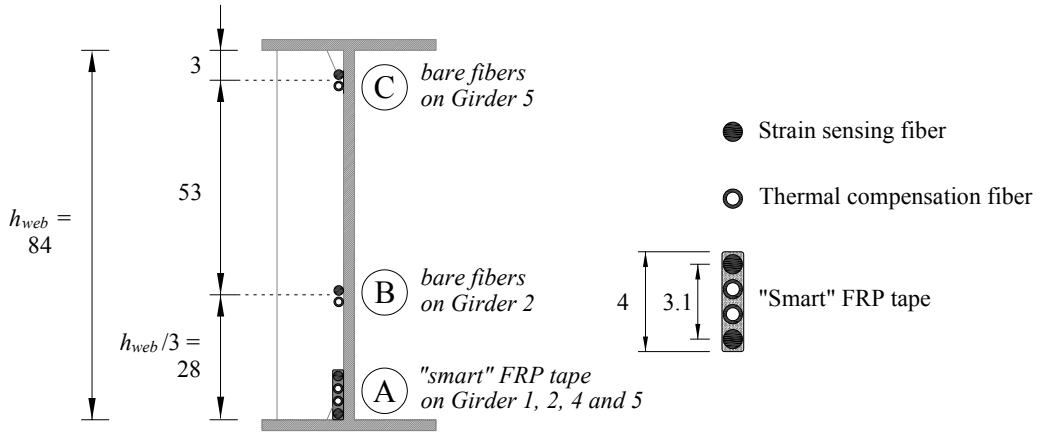

Figure 37 – Detailed location of fiber optics on girder web (not to scale, dimensions in in)

Table 3.2 – Type, identification and location of sensing elements installed

Girder	Span	Location	Fiber type	Number of Fibers × Active length (ft)	Circuit ID
1	1	A	*(Instrumented tape)*		
			tight buffer fiber	2 × 148	Ia, Ib
			loose (dry) buffer fiber	1 × 148	Ic
			loose (wet) buffer fiber	1 × 148	Id
2	1, 2*	B (h_{web}/3 = 28 in)	*(Bare fibers)*		
			loose (dry) buffer fiber	1 × (148, 137)	IIa
			tight buffer fiber	1 × (148, 137)	IIb
2	1, 2*	A	*(Instrumented tape)*		
			tight buffer fiber	1 × (148, 137)	IIIa
			loose (dry) buffer fiber	1 × (148, 137)	IIIb
4	1, 2*	A	*(Instrumented tape)*		
			tight buffer fiber	1 × (148, 137)	IVa
5	1	C (h_{web} – 3 = 81 in)	*(Instrumented tape)*		
			loose (dry) buffer fiber	1 × 148	Va
			tight buffer fiber	1 × 148	Vb
5	1, 2*	A	*(Instrumented tape)*		
			tight buffer fiber	1 × (148, 137)	VIa
			loose (dry) buffer fiber	1 × (148, 137)	VIb

** fibers are installed up to bolted joint prior to Pier 3*

The smart GFRP tape was applied over the web plate of all the girders monitored. The tape was drawn through the corner holes between the welded vertical stiffeners and the plate girder and then installed about 0.4 in above the bottom flange, in order to allow detection of a strain level reasonably close to the actual maximum attained.

Girder 1 was instrumented on Span 1 using smart tape. The tape circuit end was also lengthened for 32.8 ft after Pier 2. The additional portion installed on the web, at a distance of 15 in from the adjacent surface of the top flange (Figure 38), was used to gain additional data and therefore to estimate the position of the neutral axis. Since it was not possible to keep the tape perfectly flat in the vicinity of the cross frames, a certain disturbance of the data retrieved in those areas was expected.

Girder 2 was instrumented on Span 1 and 2. The smart tape was installed at 0.4 in from the bottom flange surface. In addition, two bare fibers, one for strain sensing and the other for thermal compensation, were bonded at 28 in from the bottom flange (*i.e.* at one third of the height of the plate web), (see Figure 39a). This was done in an attempt to evaluate the position of the neutral axis; however, the need to draw the fibers through the holes between the welded vertical stiffeners and the plate girder required several sharp bending areas of the fibers, as shown in Figure 39b, which are believed to be the cause of an undesired increase of the optical losses and significant perturbations of the strain distribution measured.

Girder 4 was instrumented on Span 1 and 2 with FRP tape only, bonded at the web base.

Girder 5 was instrumented on Span 1 and 2 with optical fiber-embedded composite tape at the web base. In addition, two bare fibers, one for strain sensing and the other for thermal compensation, were installed at 3 in from the upper flange surface (Figure 40), in order to retrieve data to estimate the temperature gradient throughout the web height, and of the strain profile, especially in the negative moment zone.

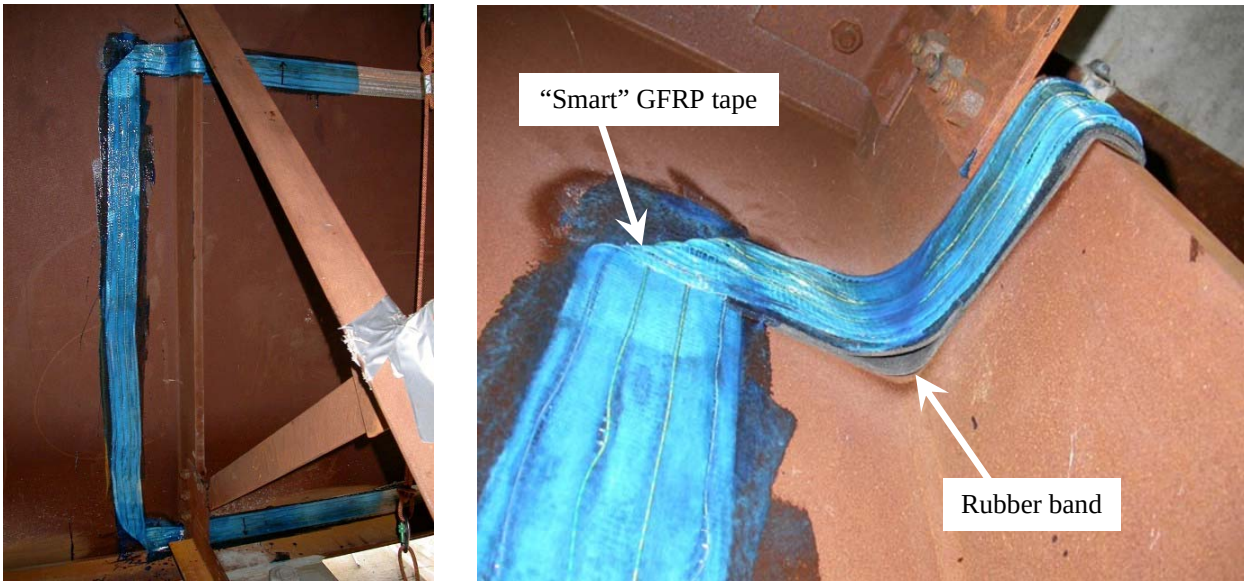

Figure 38 – Smart FRP installed on Girder 1 and folded at Pier 2 location to extend circuit

a) Smart FRP (lower blue stripe) and bare fibers (upper blue stripe)

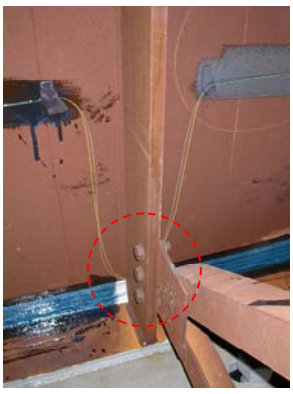

b) Bending of fibers to pass through transversal stiffeners

Figure 39 – Sensing fibers installed onto web plate of Girder 2

Figure 40 – Sensing fibers installed onto web plate of Girder 5

3.1.2 Modular cart for sensor installation

The fact that the 863 ft long bridge spans over the Osage River for about 571 ft, while the concrete deck had not been cast yet, precluded the use of a cherry-picker or any such vehicle to allow the personnel to access the desired locations along the steel girders and install the sensors. This was accomplished by the aid of a modular frame cart, designed on-purpose at the University of Missouri-Rolla, and built at the Rolla Technical Institute (Figure 41). The cart was conceived to move along the whole bridge rolling over the bottom flanges of two adjacent girders, using a set of built-in devices to by-pass the vertical stiffeners, cross frames and diaphragms at the pile locations. The vehicle is composed of three 5 ft wide and 4 ft long demountable modules, for a total working surface of about 60 ft^2. The total weight of the cart was limited to 423 lbs by extensive use of 6061-T6 aluminum profiles bolted together to form the frame, and structural GFRP pultruded planks manufactured by Strongwell Corporation (2004) as the flooring system. The transversal support members are made of AISI 1018 steel plates, which were cut to length and welded, and contain the AISI 1045 steel axles, with diameter up to 1.5 in. 3.25 in by 3.25 in polyurethane lift truck wheels with bearings were secured at one end of each axle by means of

safety pins, while a total of eight electric actuators allowed the axles to extend out of the transverse member for 18.5 in on each side of the vehicle, as shown in Figure 41c.

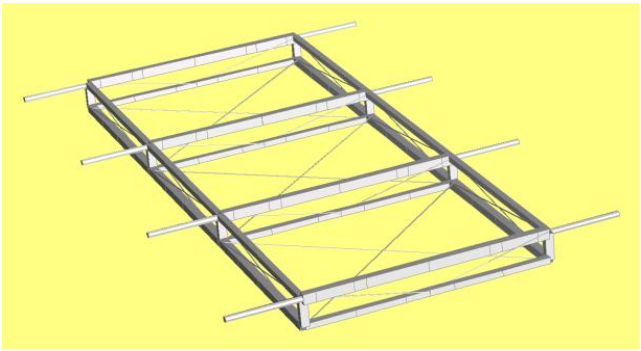

a) Schematic rendering

b) Cart frame as built

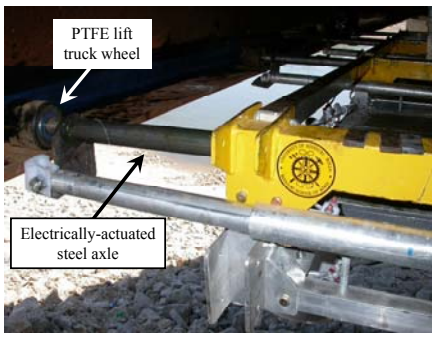

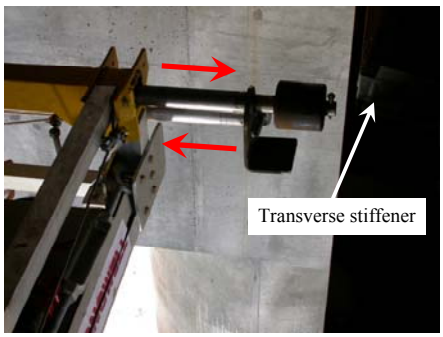

c) Electrically-actuated axles for obstacle by-passing

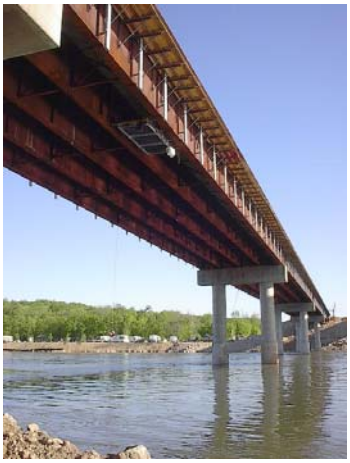

d) Along Girder 1/2, Span 2

e) Installation operations

Figure 41 – Modular frame cart for sensor installation

3.1.3 Connection and preliminary testing of the sensing elements

Upon completion of the installation procedure, the different fiber hauls were tested with the AQ8603 strain analyzer in coherent OTDR loss measurement mode. The check-up evidenced

some unwanted sources of optical loss, likely due to fiber damages which occurred during installation. The amount of optical losses in the sensing circuit is of crucial importance in BOTDR systems, since it may be highly detrimental to the strain sensitivity and accuracy. The hauls were series-connected in the field using a fiber optic fusion splicer (Figure 42), obtaining a single circuit with a total length of 3,802 ft. The solution allowed containing the total optical loss within a value of 6 dB in the first 3,366 ft from the optical test end (Figure 43), thus enabling strain measurement with a minimum accuracy of 0.004% (±40 με) on a length resolution of 6.5 ft, setting the AQ8603 analyzer for laser pulses with a length of 20 ns. Since a significant optical loss is detected before the last portion of the circuit, *i.e.* Girder 4, Location A, the correspondent measured strain profiles were expected to have a lower degree of accuracy.

Figure 42 – Optical fiber core-alignment fusion splicing field operation

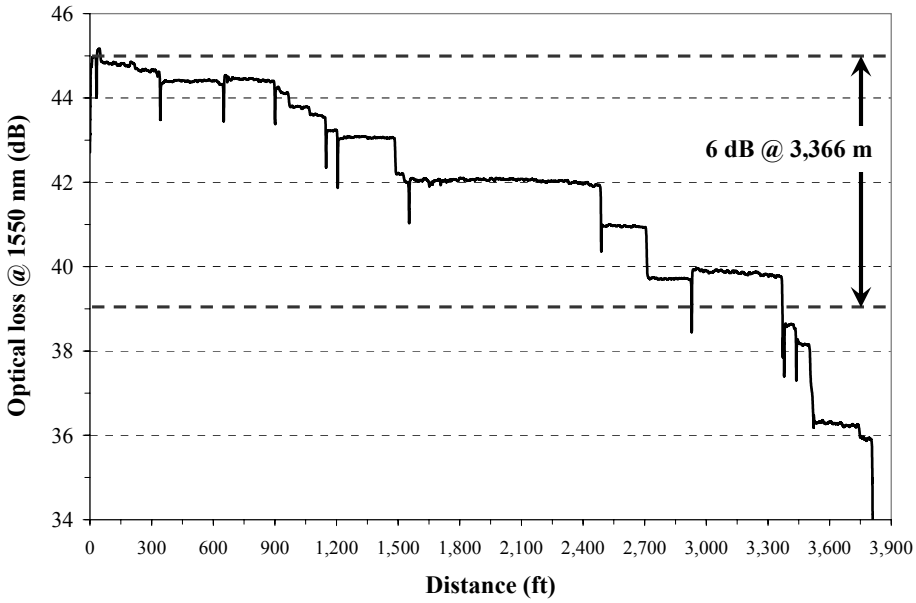

Figure 43 – Optical loss measured along sensing circuit

3.1.4 Sensing system calibration

The correlation between the strain and the Brillouin frequency shift (characteristic of the fiber used), was determined using a strain calibration fixture that allowed to induce a predetermined uniform strain in the fiber tested, over a reference length of 24.34 ft (Figure 44a).

Using the strain data collected with the calibration fixture (Figure 44b), a specific set of correction coefficients was computed for each type of fiber used, in order to improve accuracy and linearity with respect to the standard equipment settings. The best linearization was obtained for the sensing fiber embedded into the custom designed and manufactured GFRP tape, as shown in Figure 45.

In addition, since the AQ8603 unit does not allow direct temperature estimate, a suitable strain-temperature correlation was established by testing an optical fiber spool placed in an environmental chamber at different temperature levels. The results are summarized in Figure 46.

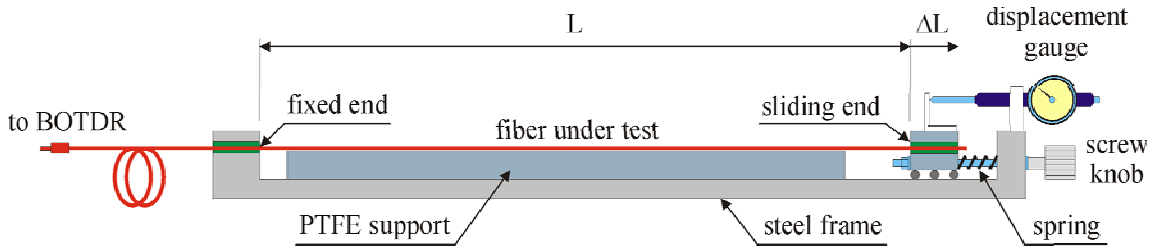

a) Schematic

b) Data recording using AQ8603 strain analyzer

Figure 44 – Strain calibration fixture

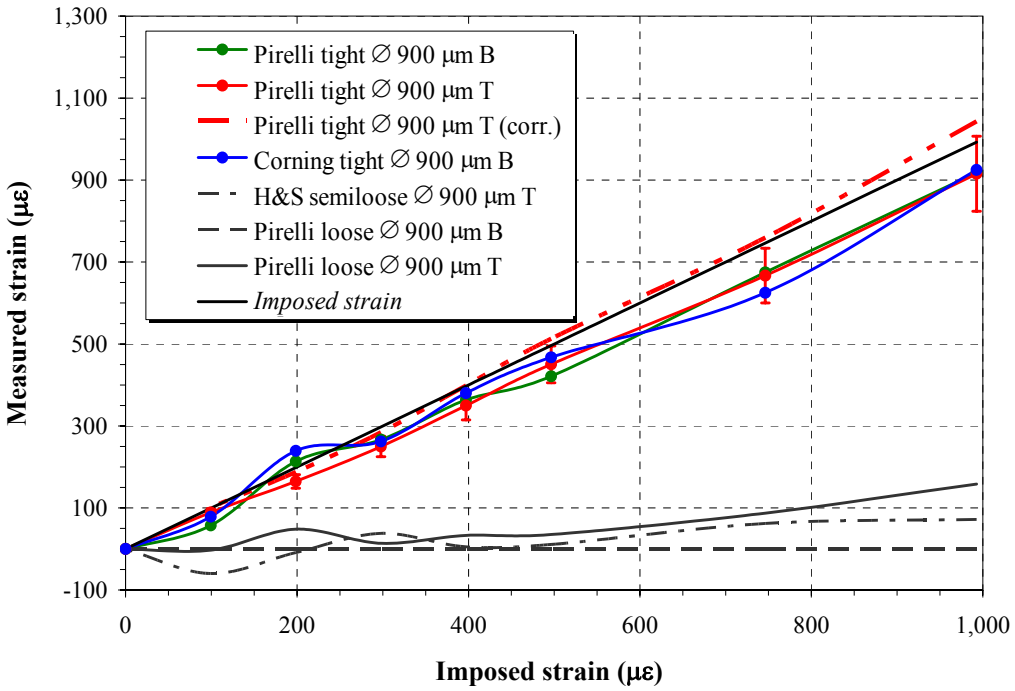

Figure 45 – Linearity of measured and imposed strain for different fibers tested

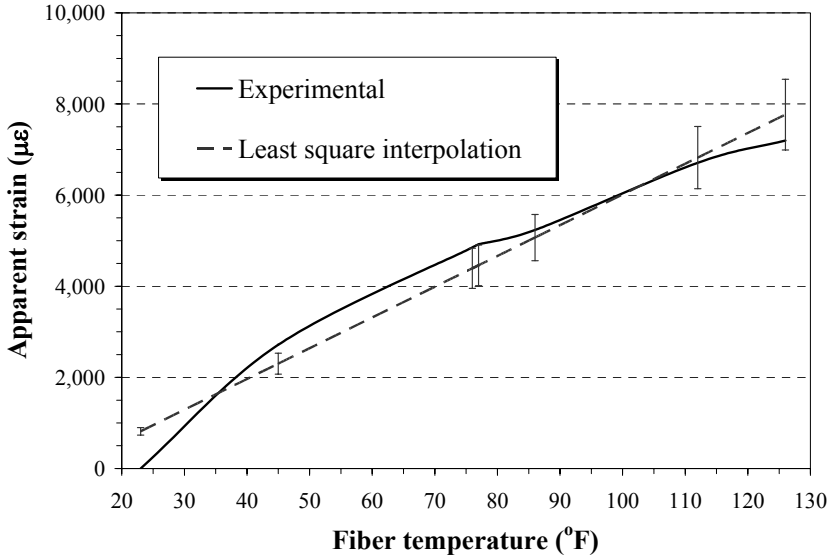

Figure 46 – Strain-temperature correlation

3.1.5 Installation of resistive strain gauges

A total of four resistive strain gauges were installed on Girder 1 and 2, in order to have a strain detection reference independent from the BOTDR system, while three additional gauges were used to evaluate the thermal drift compensation (Figure 47). Table 3.2 summarizes the type and

location of the strain gauges installed.

Table 3.3 – Type, identification and location of strain gauges installed

Gauge ID	Type*	Girder	Location	Distance from Abutment 1 (ft)
G1	TC	1	Top flange	65.5
G2	SM	1	Top flange	66.5
G3	SM	1	Bottom flange	65.5
G4	TC	1	Bottom flange	65.5
G5	SM	2	B (h_{web} / 3)	75.5
G6	SM	2	Bottom flange	75.0
G7	TC	2	Bottom flange	75.0

** TC = thermal compensation; SM = strain measurement*

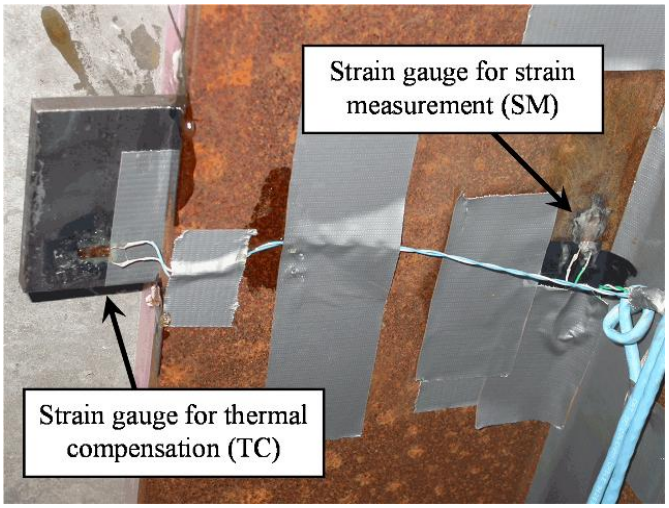

Figure 47 – Close-up of strain gauges installed on top flange of Girder 1

3.2 Test procedure

The load test procedure is described in 2.3.1. The equipment for strain measurement and recording is shown in Figure 48. The raw data exported by the strain analyzer were elaborated through proprietary software (Figure 49), in order to properly account for the distributed thermal compensation, thereby retrieving the experimental load-induced strain profile along each monitored girder. Strain data from the strain gauges were recorded continuously at a frequency of 1 Hz, using the data acquisition system shown in Figure 11.

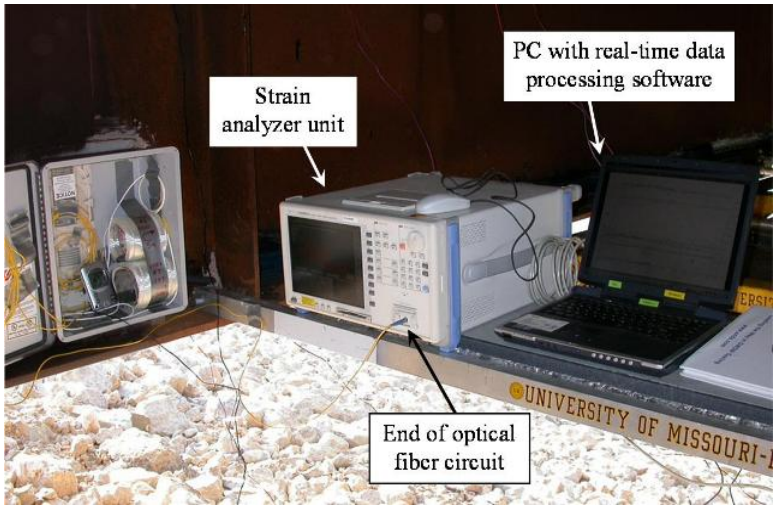

Figure 48 – Field equipment for distributed strain measurement

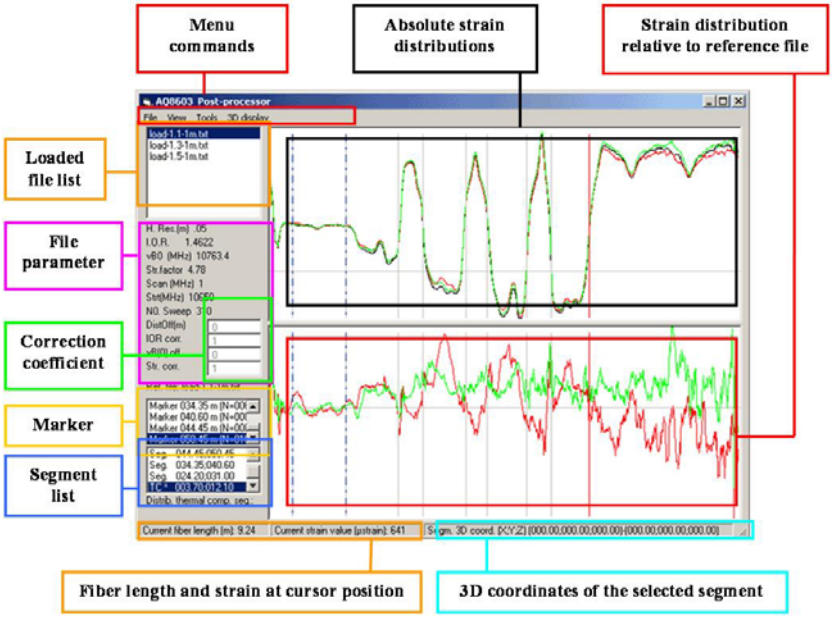

Figure 49 – Proprietary software for strain data processing

3.3 Test results

3.3.1 BOTDR strain measurement

The experimental strain profiles along the monitored girders during the load test at Stops 1, 2, 4, 7 and 8 are shown in Figure 50 to Figure 54, along with the strain gauge readings detailed in Section 3.3.2. The data from the remaining stops are currently not available due to a temporary hardware problem. The strain profile history for each monitored girder throughout the load test is provided in Appendix II.b.

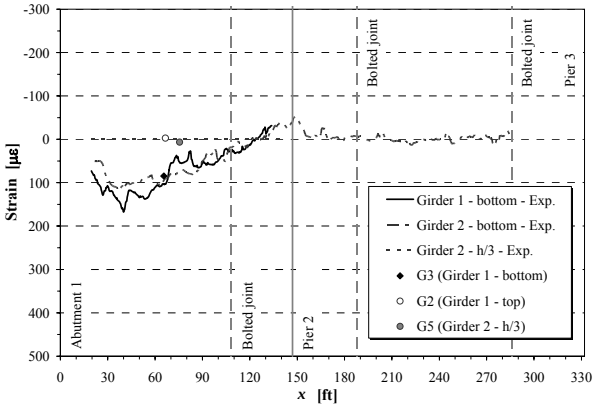

a) Girder 1 and 2

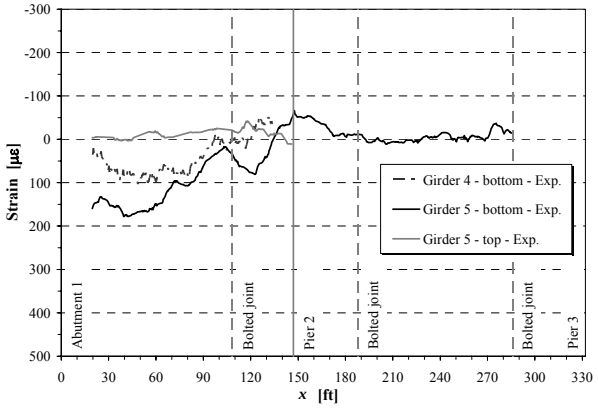

b) Girder 4 and 5

Figure 50 – Experimental strain distribution (Stop 1)

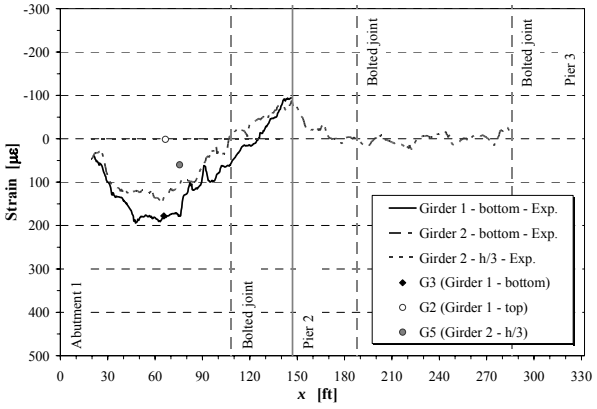

a) Girder 1 and 2

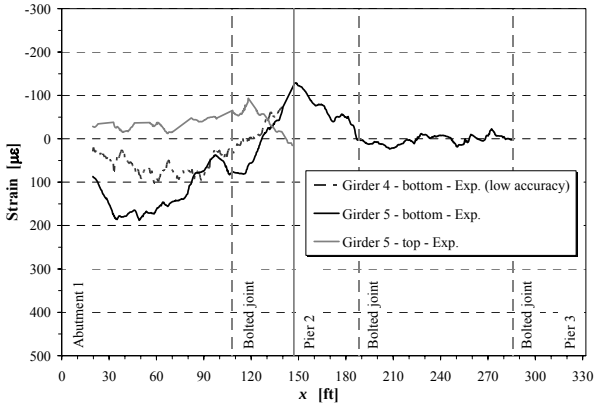

b) Girder 4 and 5

Figure 51 – Experimental strain distribution (Stop 2)

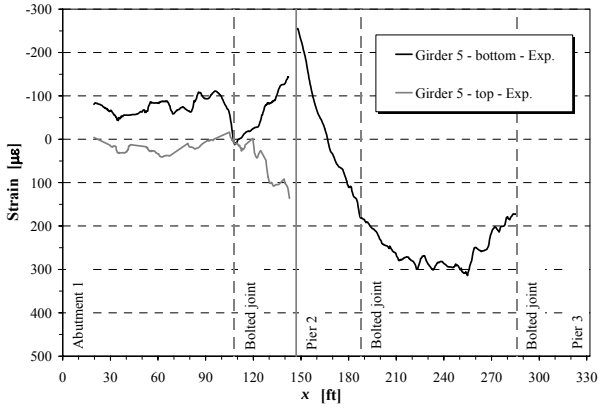

Figure 52 – Experimental strain distribution onn Girder 5 (Stop 4)

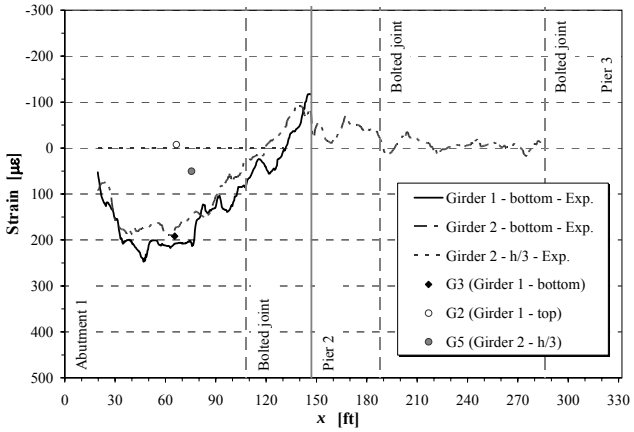

a) Girder 1 and 2

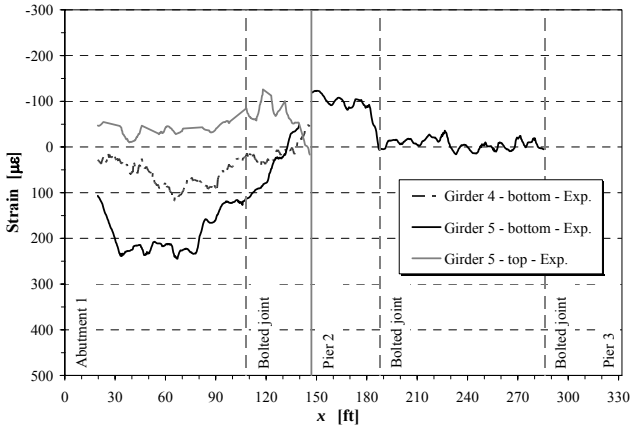

b) Girder 4 and 5

Figure 53 – Experimental strain distribution (Stop 7)

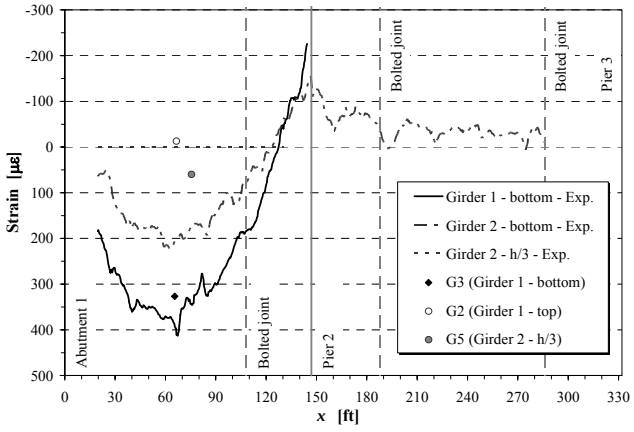

Figure 54 – Experimental strain distribution on Girder 1 and Girder 2 (Stop 8)

3.3.2 Resistive strain gauge measurements

Of the seven strain gauges installed, only G1, G2, G3, G4 and G5 worked properly during the load test. The strain reading history throughout the test and the values at each stop, computed accounting for thermal compensation, are provided in Figure 55 and Figure 56, respectively.

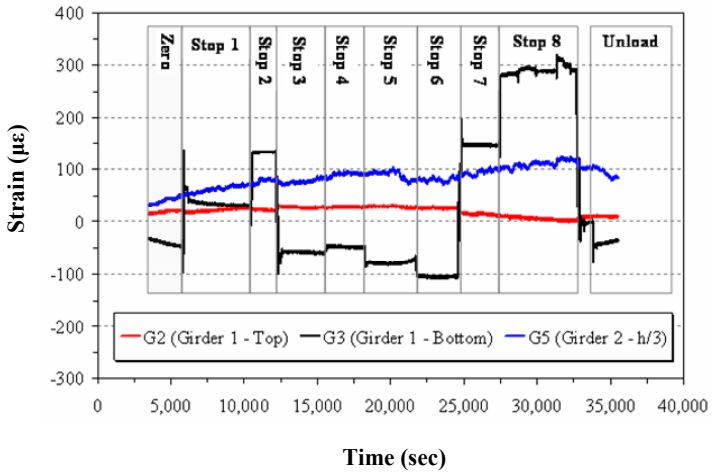

Figure 55 – Time history of strain gauge readings

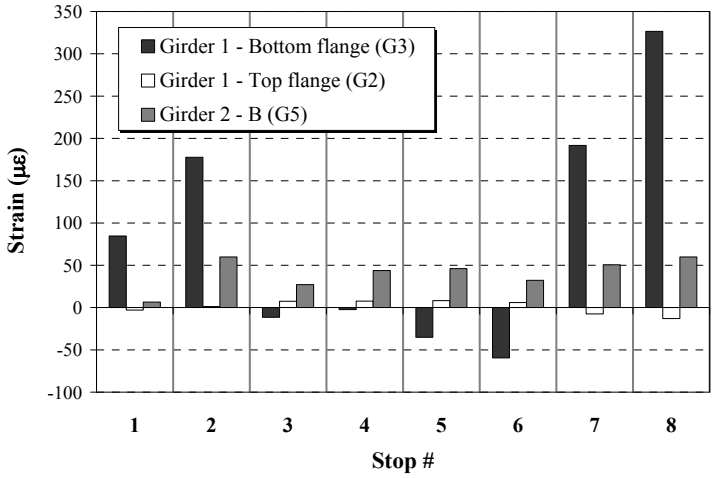

Figure 56 – Strain gauge data computed for Stop 1-8 accounting for thermal compensation

3.4 Discussion of results

The experimental results were compared with analytical strain profiles based on the AASHTO LRFD Bridge Design Specifications (AASHTO, 1998), according to the theoretical approach previously detailed in 2.3.3, pp. 27-28. Figure 57, Figure 58, Figure 59, Figure 60 and Figure 61 show the comparison between the experimental and analytical strain profiles at Stop 1, Stop 2, Stop 4, Stop 7 and Stop 8, respectively. Strain gauge readings are also included.

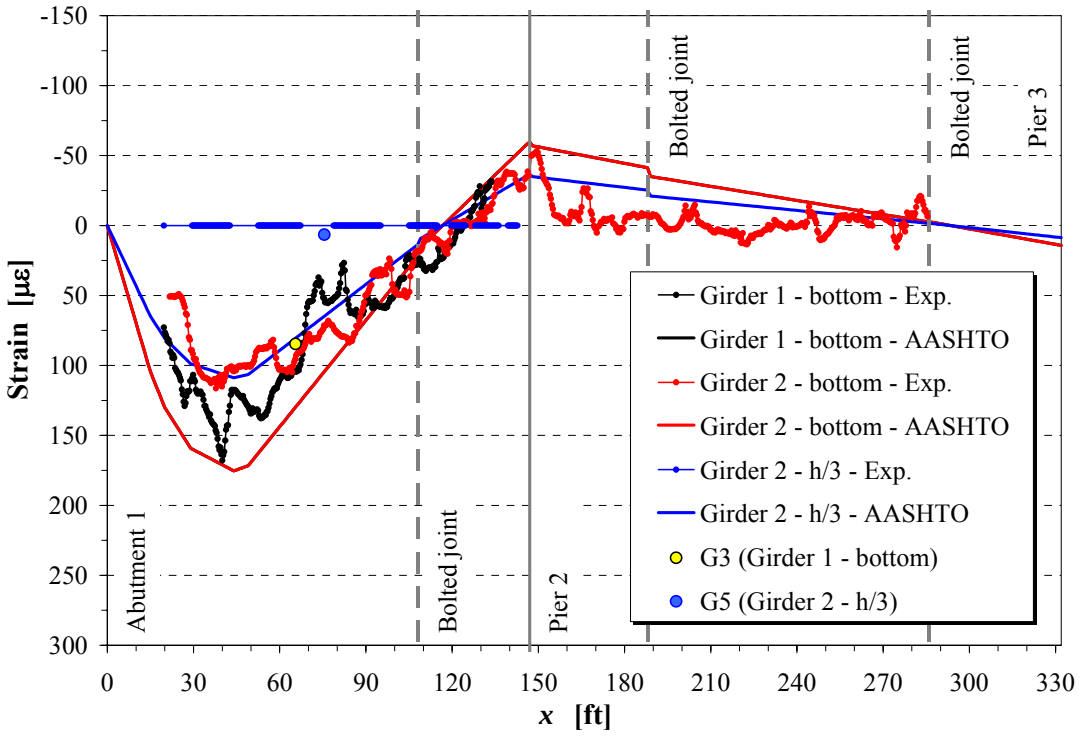

a) Girder 1 and 2

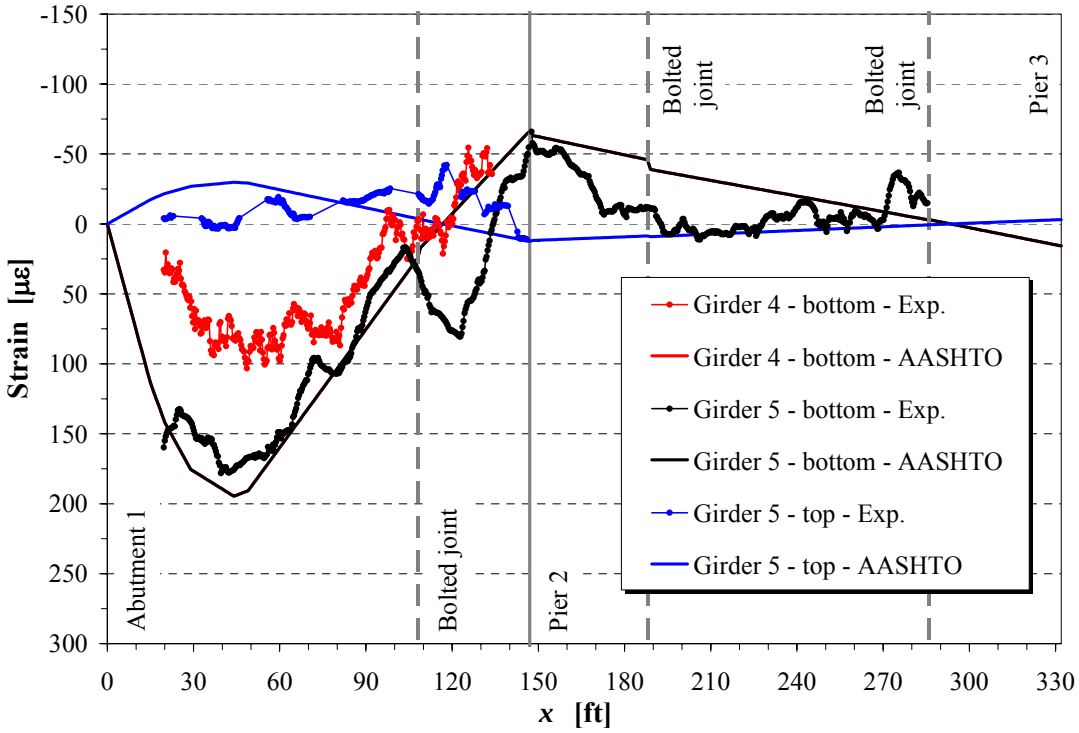

b) Girder 4 and 5

Figure 57 – Comparison between experimental and predicted strain profiles (Stop 1)

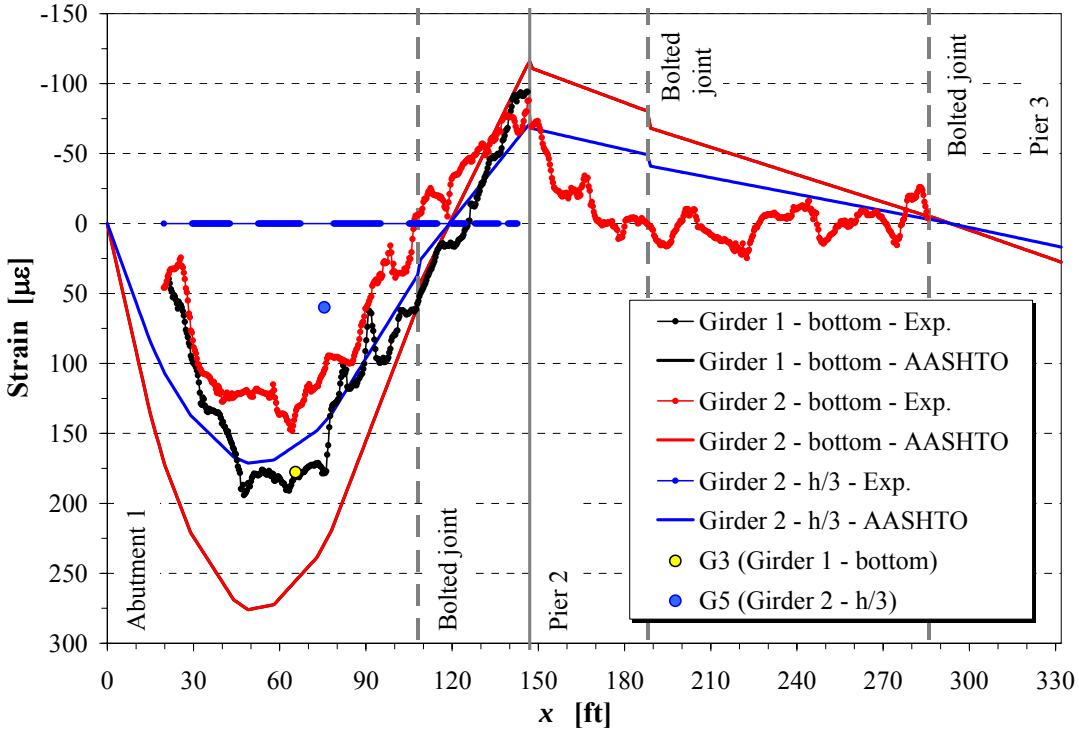

a) Girder 1 and 2

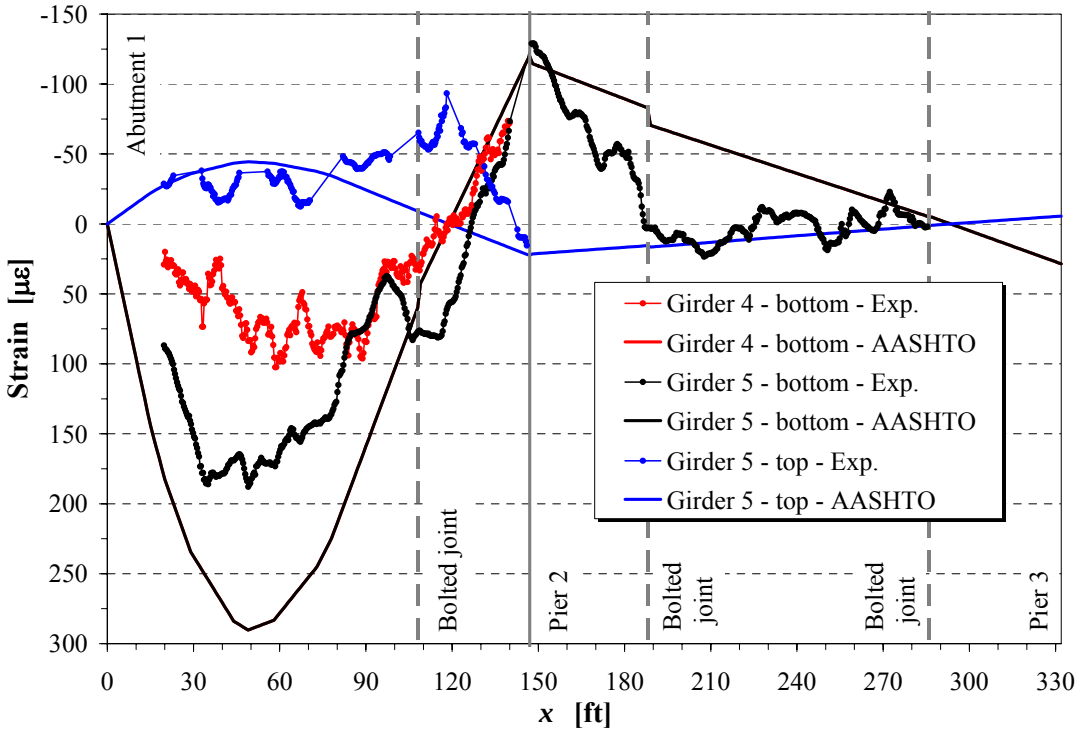

b) Girder 4 and 5

Figure 58 – Comparison between experimental and predicted strain profiles (Stop 2)

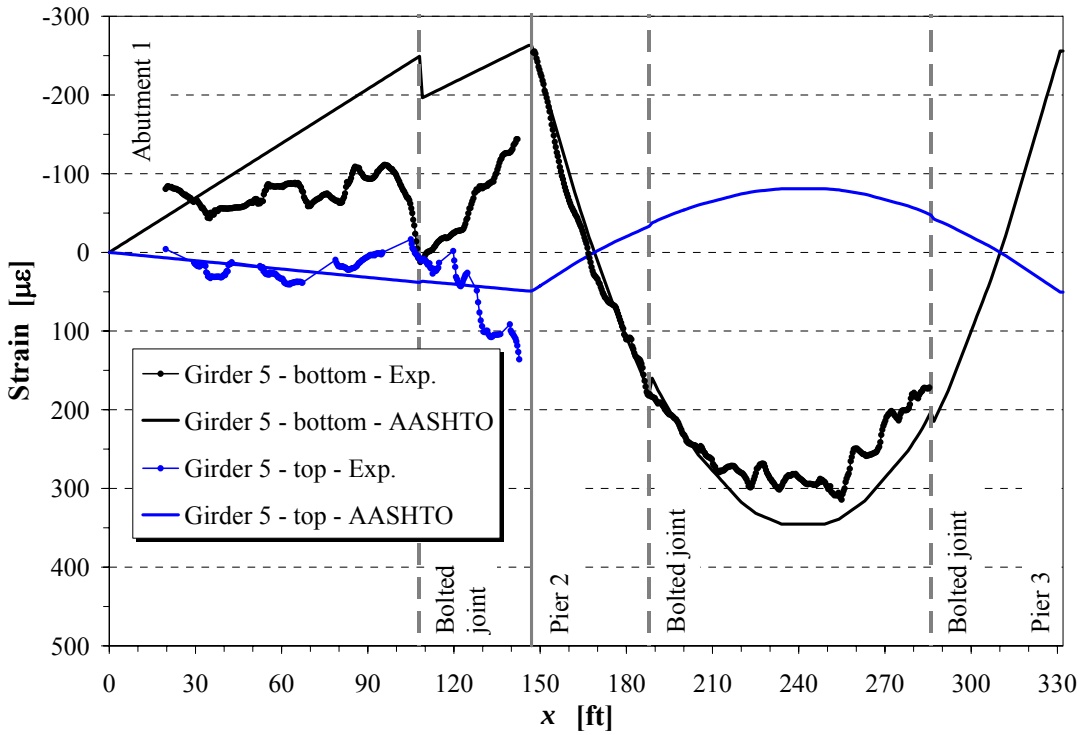

Figure 59 – Comparison between experimental and predicted strain profiles (Stop 4)

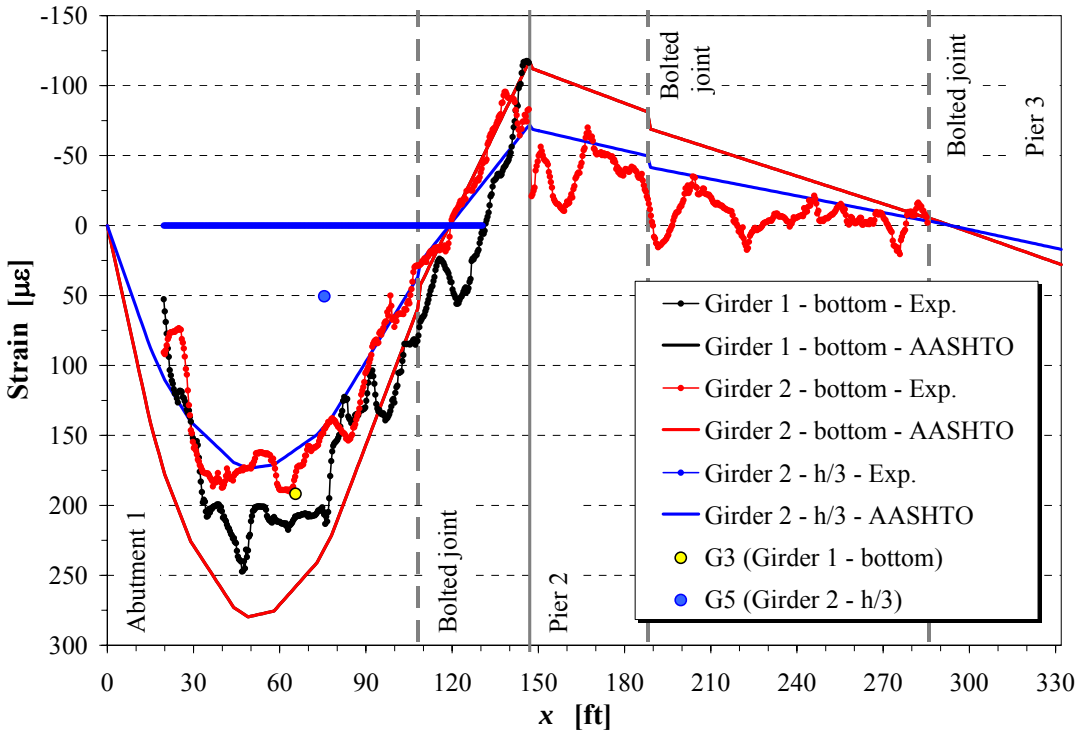

a) Girder 1 and 2

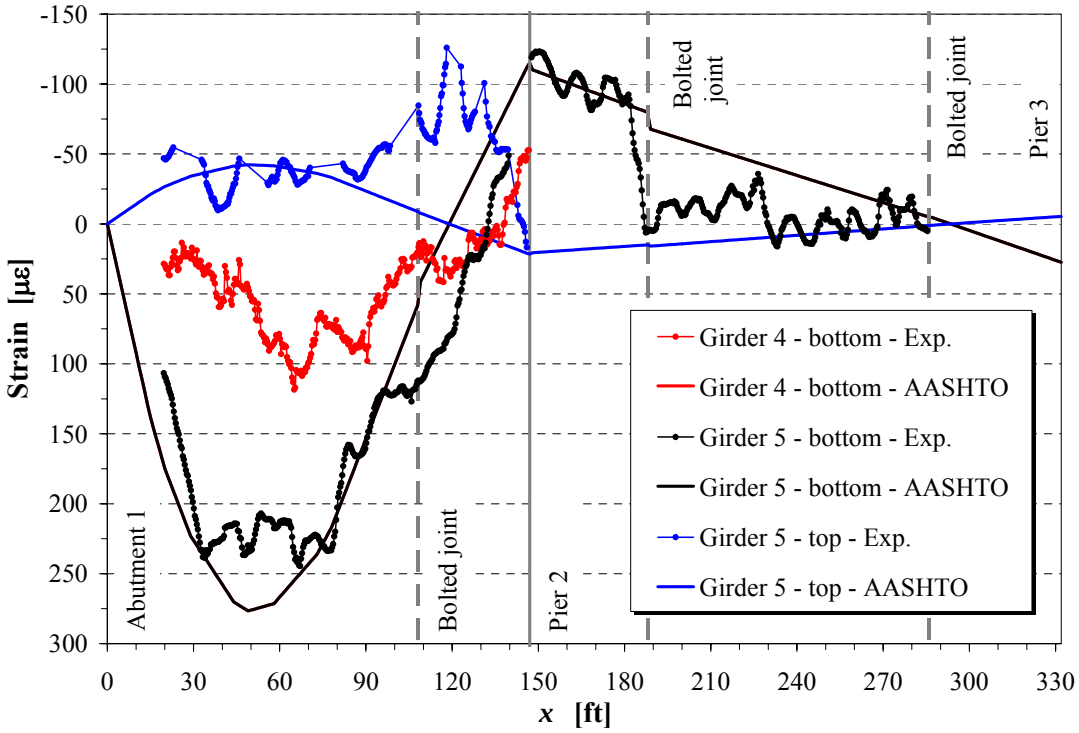

b) Girder 4 and 5

Figure 60 – Comparison between experimental and predicted strain profiles (Stop 7)

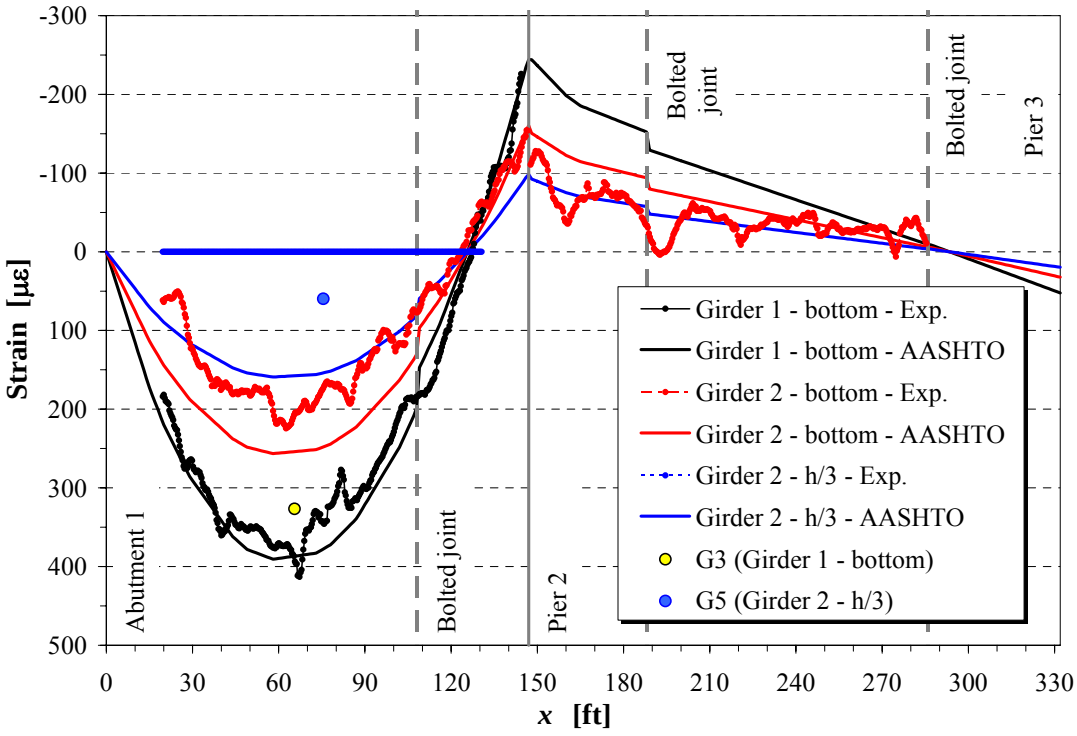

Figure 61 – Comparison between experimental and predicted strain profiles (Stop 8)

The strain readings from the optical fibers embedded in the GFRP tape fairly follow the analytical profiles in all the girders in case of one load lane (Stop 4 and 8), and in the exterior members, Girder 1 and Girder 5, in case of two load lanes (Stop 1, 2 and 7), when the distribution factor in the interior girders is not representative of the actual load test conditions. The offset is generally consistent with the strain gauge readings and the deflection results from ATS measurements, thus verifying the conservativeness of the AASHTO design provisions (1998).

As expected, the strain measurement on Girder 4, Location A (adjacent to the bottom flange), yields less accurate values, due to the significant optical loss before the interested portion of the circuit. The experimental results also point out the relation between measurement accuracy and strain level, with reliable outputs generally provided at strain levels beyond 100 με.

The BOTDR experimental data confirm the concerns raised by the ATS measurements on Girder 1. In particular, the strain profile at Stop 8 (Figure 61a) shows the clear tendency to approach the theoretical values, in accordance with the deflection results shown in Figure 32d. This indicates that the structural member ideally deforms as under a load associated with the maximum distribution factor of 0.658 load lanes accounted for. Conversely, the strain in Girder 2 at Stop 8 (Figure 61a) remains well below the analytical threshold.

Local effects, such as that at the bolted joints, may result in disturbances that affect the strain readings in a relatively large adjacent portion of the circuit, although the profiles are qualitatively correct as they often reflect the presence of local strain gradients. The issue is evident in Girder 5, Stop 1 (Figure 57b) and Stop 2 (Figure 58b) on Span 1, and Girder 5, Stop 4 (Figure 59) on

5, Stop 1 (Figure 57b) and Stop 2 (Figure 58b) on Span 1, and Girder 5, Stop 4 (Figure 59) on Span 1, whereas it seems not of concern in case of relatively high strain levels (beyond 100 με) for positive moment regions. This suggests that localized inconsistencies may be essentially due to initial fiber misalignment and/or local disbond, with reduced effect as the fibers are progressively stretched.

It is finally noticed that the data retrieved from the bare fibers did not have the same quality of that from the GFRP tape, in particular in Girder 2, Location B (at $h_{web}/3$, Figure 37), where practically zero strain was detected. This may be principally due to the presence of several vertical circuit portions, sometimes partially unbonded, in the vicinity of the transverse stiffeners, which likely caused undesired perturbations in the signals detected.

4. CONCLUSIONS

Conclusions based on the deflection measurement *via* ATS during pouring of the deck slab and diagnostic load test, strain measurement *via* BOTDR during the load test, and comparison with analytical results based on the AASHTO LRFD Bridge Design Specifications (1998), can be summarized as follows:

1. The structural assessment confirms the safety of the bridge, since the experimental deflection and strain results were found to be smaller than the theoretical values determined according to the design provisions (AASHTO, 1998);
2. A significant drop in the behavior of one of the exterior girders (Girder 1) was assessed, with differences in the Span 1 midspan deflection between Girder 1 and Girder 5 of the order of 30%, under similar load conditions. In the case of the load test, such difference cannot be justified considering concurrent factors that typically affect the experimental results. A preliminary explanation may account for a possible alteration of the structural response as a consequence of the falling of the steel girder during erection of the superstructure. The issue calls for further verification and monitoring during the life of the bridge;
3. Experimental results from both techniques employed fairly describe the global response of the bridge both in terms of deflections and strains, and were consistent with each other;
4. ATS confirms its cost-effectiveness for deflection measurement. The fact that the technology allows for non-contact measurement significantly enhances its versatility;
5. BOTDR is a promising, novel method for global structural assessment, with the unique ability to detect the distributed strain along a structural member. In particular, the adhesively bonded custom-made GFRP tape with embedded optical fibers for strain measurement provided a far better performance than bare fibers.

5. REFERENCES

American Association of State Highway and Transportation Officials (1996), "LFD Standard Specifications", 16th ed., AASHTO, Washington, D.C.

American Association of State Highway and Transportation Officials (1998), "LRFD Bridge Design Specifications", 2nd ed., AASHTO, Washington, D.C.

American Association of State Highway and Transportation Officials (2002), "Standard Specifications for Highway Bridges", 17th ed., AASHTO, Washington, D.C.

Azizinamini, A., Barth, K. E., Dexter, R. and Rubeiz, C. (2004), "High Performance Steel: Research Front – Historical Account of Research Activities", *ASCE Journal of Bridge Engineering*, 9[3], pp. 212-217.

Barker, M.G. and Schrage, S.D. (2000), "High Performance Steel: Design and Cost Comparisons", *Modern Steel Construction*, American Institute of Steel Construction, 16, pp. 35-41.

Barnoski, M.K. and Jensen, S.M. (1976), "Fiber Waveguides: A Novel Technique for Investigating Attenuation Characteristics", *Applied Optics*, 15[9], pp. 2112-2115.

Barth, K.E., Roeder, C.W., Christopher, R.A. and Wu, H. (2001), "Evaluation of Live Load Deflection Criteria for I-shaped Steel Bridge Design Girders", *Proc. International Conference on High Performance Materials in Bridges*, Kona, HI, Jul. 29 – Aug. 3, 2001, A. Azizinamini, A. Yakel and M. Abdelrahman, eds., American Society of Civil Engineers, pp. 193-208.

Bastianini, F., Cargnelutti, M., Di Tommaso, A. and Toffanin, M. (2003), "Distributed Brillouin Fiber Optic Strain Monitoring Applications in Advanced Composite Materials", *Proc. SPIE*, 5057, pp. 478-485.

Brillouin, L. (1922), "Diffusion de la Lumière et des Rayonnes X par un Corps Transparent Homogéne; Influence del'Agitation Thermique", *Annales des Physique*, 17, pp. 88-122.;

Casadei, P. and Nanni, A. (2003), "In-Situ Load Testing of Reinforced Concrete Structures: Case Studies", *Proc. Concrete Technology Today*, Singapore, Vol. 3, pp. 10-16.

Casas, J.R. and Cruz, P.J.S. (2003), "Fiber Optic Sensors for Bridge Monitoring", *ASCE Journal of Bridge Engineering*, 8[6], pp. 362-373.

Chajes, M.J., Mertz, D.R. and Commander, B. (1997), "Experimental Load Rating of a Posted Bridge", *ASCE Journal of Bridge Engineering*, 2[1], pp. 1-10.

Clingenpeel, B.F. and Barth, K.E. (2003), "Design Optimization Study of a Three-span Continuous Bridge Using HPS70W", *AISC Engineering Journal*, 39[3], pp. 121-126.

Deza, U. (2004) "Evaluation of the In-Service Performance of Bridge Decks Built with Fiber Reinforced Polymer (FRP) Composite Systems", Master Thesis, University of Missouri-Rolla, Rolla, MO, U.S.A.

Federal Highway Administration Bridge Programs NBI Data (2004), "Material Type of Structure by State", *http://www.fhwa.dot.gov/bridge/mat03.xls*.

Galati, N., Casadei, P. and Nanni, A. (2004), "In-situ Load Testing of Bridge A6101

Lexington, MO", CIES Report 04-002, University of Missouri-Rolla, Rolla, MO, U.S.A.

Hill, C.D. and Sippel, K.D. (2002), "Modern Deformation Monitoring: a Multi Sensor Approach", *Proc. XXII FIG International Congress*, International Federation of Surveyors, April 19-22, 2002, Washington, D.C., 12 pp., *http://www.fig.net/pub/fig_2002/Ts6-3/TS6_3_hill _sippel.pdf*.

Hill, K.O., Johnson, D.C. and Kawasaki, B.S. (1976), "CW Generation of Multiple Stokes and Anti-Stokes Brillouin-Shifted Frequencies", *Applied Physics Letters*, 29, pp. 185-187.

Horiguchi, T., Kurashima, T. and Tateda, M. (1989), "Tensile Strain Dependence of Brillouin Frequency Shift in Silica Optical Fibers", *IEEE Photonics Technology Letters*, 1[5], pp. 107-108.

Horiguchi T., Kurashima, T. and Koyamada, Y. (1994), "1-m Spatial Resolution Measurement of Distributed Brillouin Frequency Shift in Single-Mode Fibers", *Proc. NIST/IEEE Symposium on Optical Fiber Measurements*, Boulder, CO, Sep. 1994, pp. 73-76.

Horton, R., Power, E., Van Ooyen, K. and Azizinamini, A. (2000), "High Performance Steel Cost Comparison Study.'' *Proc. Steel Bridge Design and Construction for the New Millennium with Emphasis on High Performance Steel*, Baltimore, MD, pp. 120-137.

Komatsu, K., Fujihashi, K. and Okutsu, M. (2002), "Application of the Optical Sensing Technology to the Civil Engineering Field with Optical Fiber Strain Measurement Device (BOTDR)", presented at the *SPIE Smart Sensor Technology and Measurement Systems Conference (SPIE 4694)*, San Diego, CA, Mar. 17-21, 2002.

Kuhlmann, H. and Gläser, A. (2002), "Investigation of New Measurement Techniques for Bridge Monitoring", *Proc. 2nd Symposium on Geodesy for Geotechnical and Structural Engineering*, Berlin, Germany, pp. 123-132, *http://www.uni-stuttgart.de/iagb/publikation/ newmeasure_bridge.pdf*.

Leica Geosystems, Automated High Performance Total Station TCA2003, *http://www.leica-geosystems.com/surveying/product/totalstations/tc2003.htm*.

Lynch, R.J. (2004), "Provisional Design Guide in AASHTO Language for FRP Bridge Strengthening", Master Thesis, University of Missouri-Rolla, Rolla, MO, U.S.A.

McDermott, J.F. (1969), "Local Plastic Buckling of A514 Steel Members", *ASCE Journal of the Structural Division*, 5[9], pp. 1837-1850.

Meng, X. (2002), "Real-Time Bridge Deflection and Vibration Monitoring Using an Integrated GPS/Accelerometer/Pseudolite System", *Proc. 11th FIG Symposium on Deformation Measurements*, Santorini, Greece, May 25-28, 2003, *www.fig.net/commission6/santorini/I-Monitoring%20Static%20and%20 Dyn/I5.pdf*.

Merkle, W.J. (2004), "Load Distribution and Response of Bridges Retrofitted with Various FRP Systems", Master Thesis, University of Missouri-Rolla, Rolla, MO, U.S.A.

Pelous, J. and Vacher, R. (1975), "Thermal Brillouin Scattering Measurements of the Attenuation of Longitudinal Hypersounds in Fused Quartz from 77 to 300 K", *Solid State Communications*, 16[3], p. 279.

Radovanovic, R.S. and Teskey, W.F. (2001), ''Dynamic Monitoring of Deforming

Structures: GPS versus Robotic Tacheometry Systems", *Proc. 10th FIG Symposium on Deformation Measurements*, Orange, CA, May 19-22, 2001, *http://rincon.gps.caltech.edu/FIG10sym/pdf/Session%20II_Paper%204.pdf*.

Roeder, C.W., Barth, K.E. and Bergman, A. (2004), ''Effect of Live-Load Deflections on Steel Bridge Performance", *ASCE Journal of Bridge Engineering*, 9[3], pp. 259-267.

Roeder, C.W., Barth, K.E., Bergman, A. and Christopher, R.A. (2001), "Improved Live-Load Deflection Criteria for Steel Bridges", *NCHRP Interim Report No. 20-07/133*, National Cooperative Highway Research Program, Washington, D.C.

Strongwell Corporation (2004), Fiberglass Flooring and Decking System brochure, *http://www.strongwell.com/PDFfiles/SafdeckSafplank/FlooringandDecking0304.pdf*.

Thomas, P.J., Rowell, N.L., van Driel, H.M. and Stegeman, G.I. (1979), "Normal Acoustic Modes and Brillouin Scattering in Single-Mode Optical Fibers", *Physical Review B*, 19, pp. 4986-4998.

Watson Bowman Acme Corporation (2004), Wabo® MBrace Saturant Data Sheet, *http://www.wbacorp.com/downloads/DataSheets/Composites/MBraceSaturant.pdf*.

Yariv, A. (1989), "Quantum Electronics", 3rd ed., John Wiley & Sons.

APPENDIX I – LOAD TEST STOPS

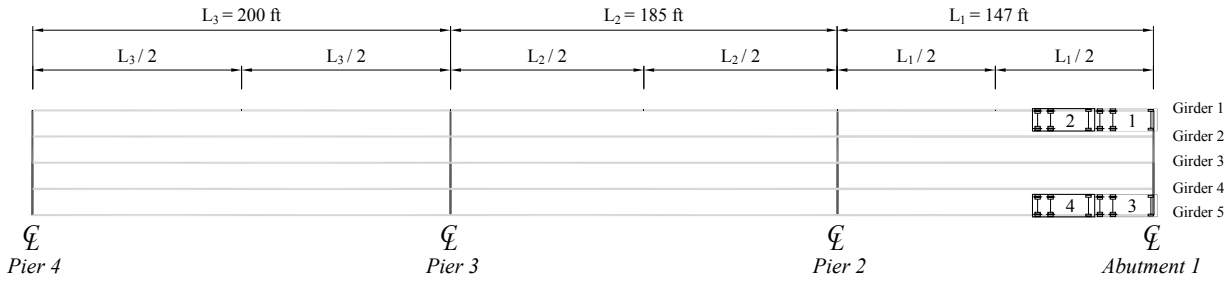

Stop 1

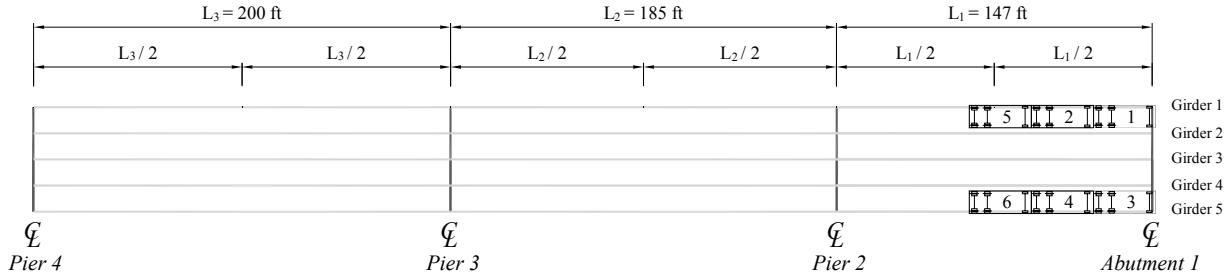

Stop 2

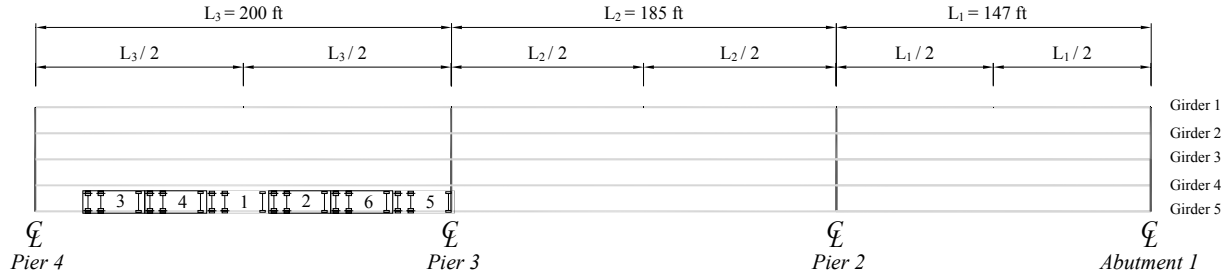

Stop 3

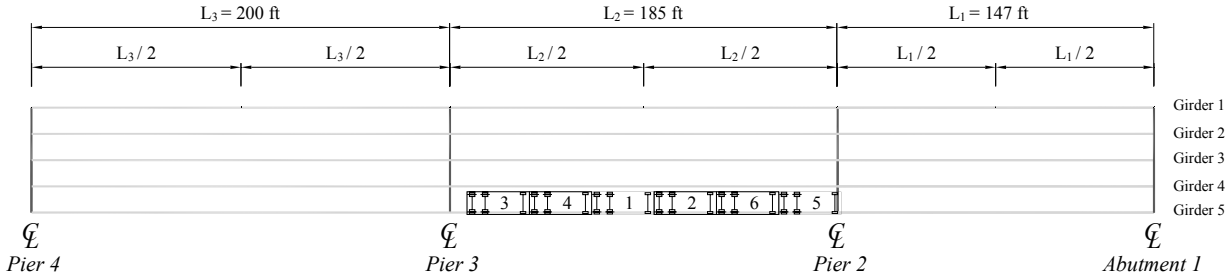

Stop 4

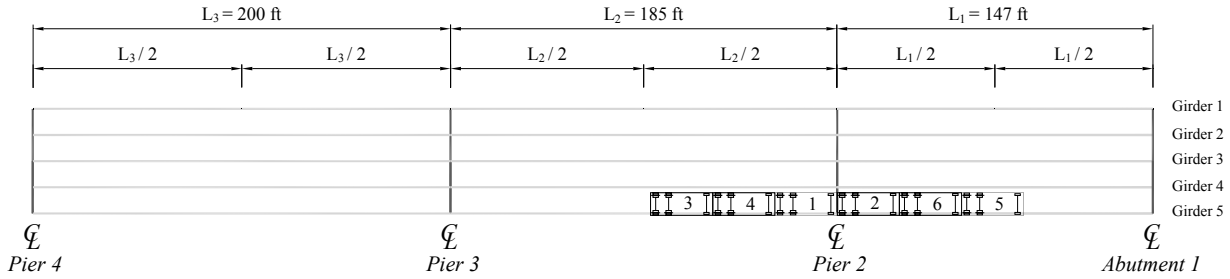

Stop 5

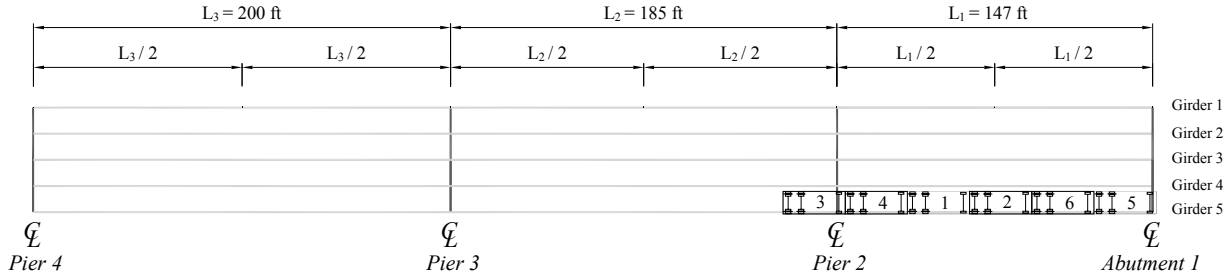

Stop 6

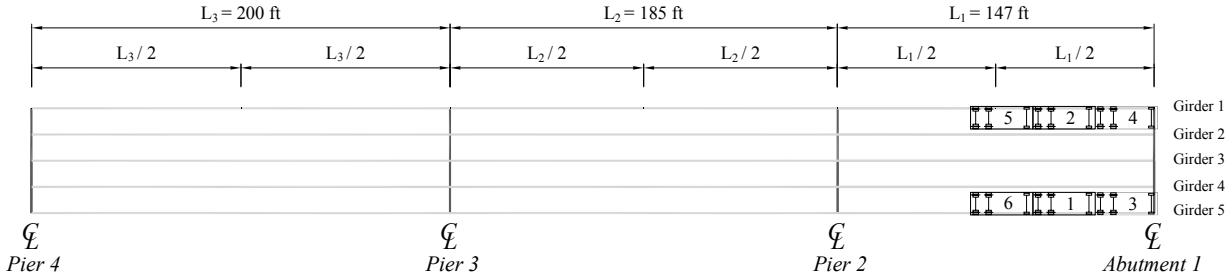

Stop 7

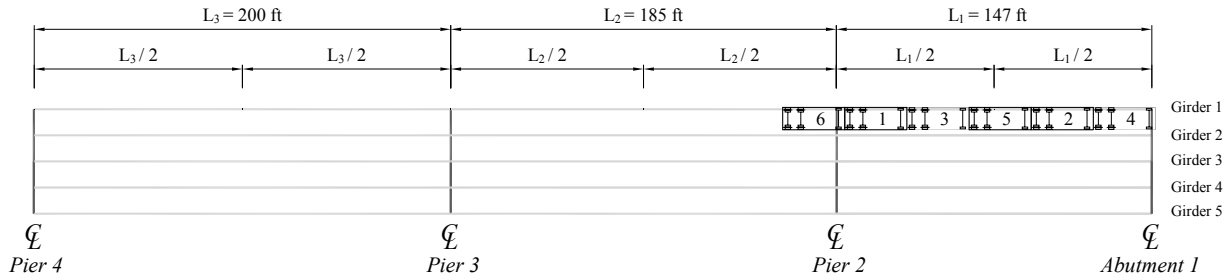

Stop 8

APPENDIX II – RAW DATA

II.a Deflection data (ATS)

Concrete-deck pouring					
x **[ft]**	***1 1/4 spans*** **[in]**	***2 spans*** **[in]**	***2 3/4 spans*** **[in]**	***4 spans*** **[in]**	***5 spans*** **[in]**
Girder 1					
3.0	1.74E-02	2.53E-02	8.27E-03	6.57E-02	-9.76E-02
50.0	1.02E-01	1.26E-01	-9.96E-03	5.16E-01	-1.13E+00
73.5	1.16E-01	1.32E-01	-1.02E-01	4.98E-01	-1.19E+00
111.0	5.50E-02	6.75E-02	-1.46E-01	3.23E-01	-5.93E-01
143.0	1.97E-04	-2.09E-02	-3.48E-02	6.76E-02	-3.87E-02
Girder 2					
73.5	7.14E-02	1.39E-01	-1.04E-01	7.11E-01	-1.05E+00
Girder 3					
3.0	1.22E-02	2.75E-02	4.17E-02	1.30E-01	-2.22E-02
50.0	2.22E-02	1.42E-01	-2.43E-02	9.12E-01	-9.54E-01
73.5	2.22E-02	1.35E-01	-1.51E-01	9.00E-01	-1.03E+00
111.0	9.80E-03	6.55E-02	-1.72E-01	6.15E-01	-4.95E-01
143.0	7.40E-03	1.51E-02	-2.76E-02	8.24E-02	-2.30E-02
188.0	-2.50E-02	-6.09E-02	3.75E-01	-1.21E+00	-6.01E-01
234.5	-4.62E-02	-1.34E-01	9.67E-01	-1.77E+00	-1.14E+00
Girder 4					
73.5	-3.90E-02	1.21E-01	-7.80E-02	1.12E+00	-8.82E-01
Girder 5					
3.0	1.26E-02	1.59E-02	N.A.	N.A.	N.A.
50.0	-1.19E-01	8.03E-02	-1.26E-01	1.11E+00	-8.62E-01
73.5	-9.86E-02	8.47E-02	-1.70E-01	1.19E+00	-8.98E-01
111.0	-4.94E-02	5.15E-02	-1.93E-01	8.04E-01	-4.27E-01
143.0	1.97E-04	2.11E-02	-5.35E-03	1.00E-01	9.13E-03
151.0	1.62E-02	5.51E-03	4.89E-02	-1.21E-01	-1.15E-02
188.0	5.86E-02	-6.25E-02	4.01E-01	-1.34E+00	-6.66E-01
234.5	5.79E-03	-1.67E-01	9.08E-01	-2.03E+00	-1.35E+00

Diagnostic load test								
x **[ft]**	***Stop 1*** **[in]**	***Stop 2*** **[in]**	***Stop 3*** **[in]**	***Stop 4*** **[in]**	***Stop 5*** **[in]**	***Stop 6*** **[in]**	***Stop 7*** **[in]**	***Stop 8*** **[in]**
Girder 1								
3.0	-5.56E-02	-9.90E-02	-1.78E-02	-1.26E-02	7.64E-03	7.95E-03	-6.41E-02	-1.55E-01
50.0	-4.99E-01	-8.19E-01	-1.50E-01	-2.11E-01	-1.24E-01	4.67E-02	-8.29E-01	-1.37E+00
73.5	-4.79E-01	-8.25E-01	-1.37E-01	-1.95E-01	-6.80E-02	7.81E-02	-8.48E-01	-1.50E+00
111.0	-2.20E-01	-4.75E-01	-7.78E-02	-1.23E-01	-6.54E-02	5.33E-02	-4.57E-01	-9.85E-01
143.0	1.34E-03	-2.92E-02	2.30E-02	1.08E-02	3.80E-02	2.83E-02	-1.57E-02	-1.26E-01
Girder 2								
73.5	-4.19E-01	-7.17E-01	-1.00E-01	5.76E-02	-4.24E-02	-1.76E-01	-7.47E-01	-9.57E-01
Girder 3								
3.0	-1.64E-02	-5.19E-02	9.72E-03	4.98E-02	3.40E-02	-1.46E-02	-4.34E-02	-3.03E-02
50.0	-3.67E-01	-6.07E-01	-5.47E-02	2.20E-01	-3.07E-02	-3.88E-01	-6.03E-01	-4.57E-01
73.5	-3.84E-01	-6.41E-01	-6.20E-02	2.79E-01	-4.46E-02	-4.35E-01	-6.55E-01	-5.18E-01
111.0	-2.18E-01	-3.76E-01	-4.75E-02	2.34E-01	7.09E-03	-2.78E-01	-3.80E-01	-3.27E-01
143.0	3.94E-05	-3.43E-02	6.30E-04	6.14E-02	2.76E-02	-3.00E-02	-2.16E-02	-2.62E-02
188.0	1.59E-01	2.27E-01	1.38E-01	-3.82E-01	-1.22E-01	1.61E-01	2.23E-01	1.82E-01
234.5	1.75E-01	2.50E-01	2.81E-01	-6.56E-01	-2.21E-01	1.76E-01	2.44E-01	1.86E-01
Girder 4								
73.5	-5.26E-01	-7.62E-01	-1.65E-01	3.38E-01	-2.26E-01	-8.98E-01	-7.62E-01	-2.36E-01
Girder 5								
3.0	-4.68E-02	-7.66E-02	-8.66E-03	7.24E-02	-1.46E-03	-9.99E-02	-4.90E-02	2.30E-02
50.0	-5.97E-01	-8.10E-01	-1.48E-01	5.19E-01	-2.53E-01	-1.10E+00	-7.35E-01	1.26E-01
73.5	-5.23E-01	-7.72E-01	-9.66E-02	7.16E-01	-2.23E-01	-1.17E+00	-7.05E-01	1.88E-01
111.0	-3.06E-01	-4.65E-01	-1.23E-01	5.90E-01	-1.34E-01	-8.24E-01	-4.20E-01	1.21E-01
143.0	2.99E-03	-2.75E-02	-6.14E-03	9.46E-02	5.87E-03	-7.16E-02	-2.47E-02	2.07E-02
151.0	4.40E-02	3.18E-02	3.53E-02	-7.43E-02	-3.19E-02	4.79E-02	4.31E-02	6.61E-03
188.0	1.38E-01	1.90E-01	2.27E-01	-1.11E+00	-5.19E-01	2.85E-01	1.67E-01	-6.39E-02
234.5	1.37E-01	1.90E-01	4.91E-01	-1.85E+00	-7.61E-01	2.61E-01	1.38E-01	-1.08E-01

II.b Strain data (BOTDR)

Girder 1 (Location A, Table 3.2)

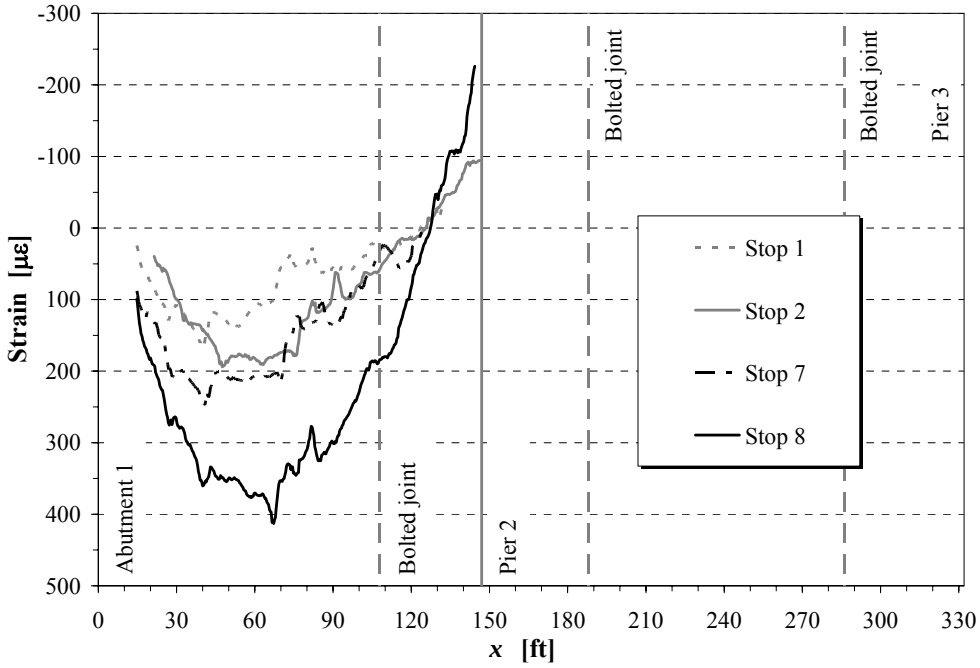

Girder 2 (Location A, Table 3.2)

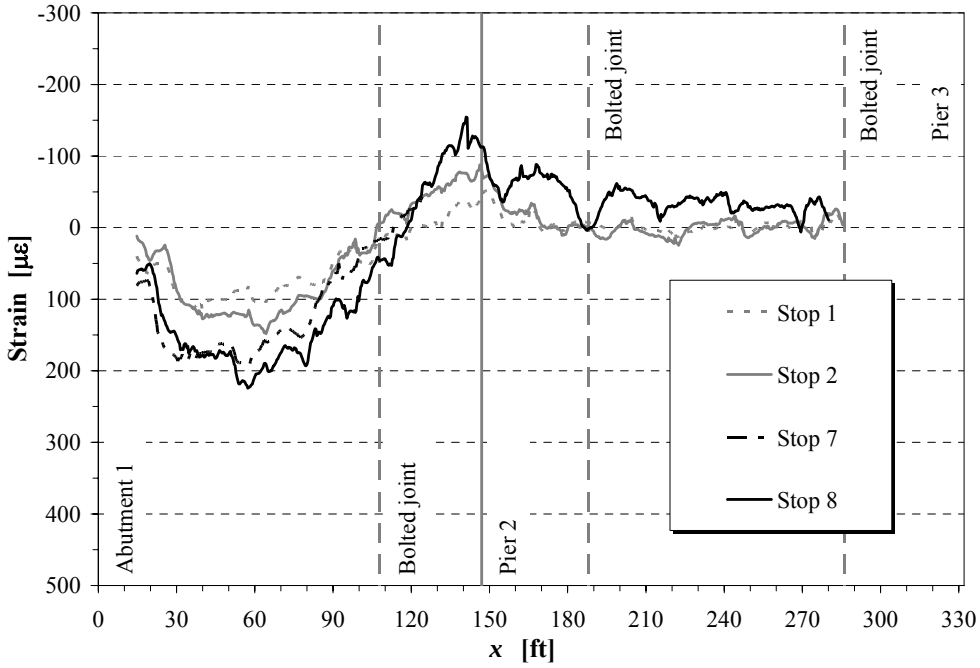

Girder 2 (Location B, Table 3.2)

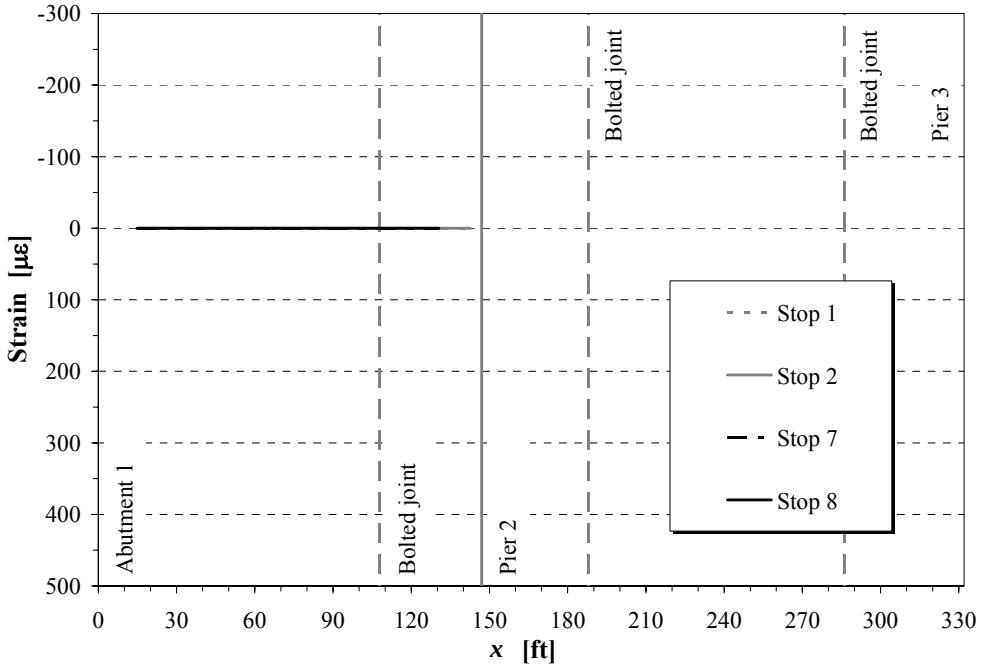

Girder 4 (Location A, Table 3.2)

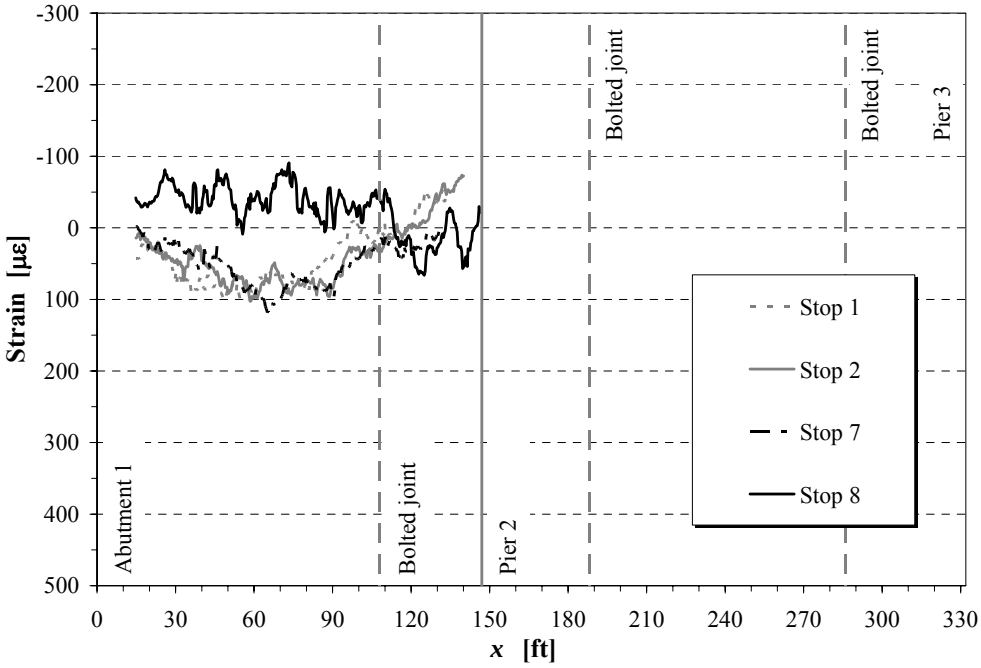

Girder 5 (Location A, Table 3.2)

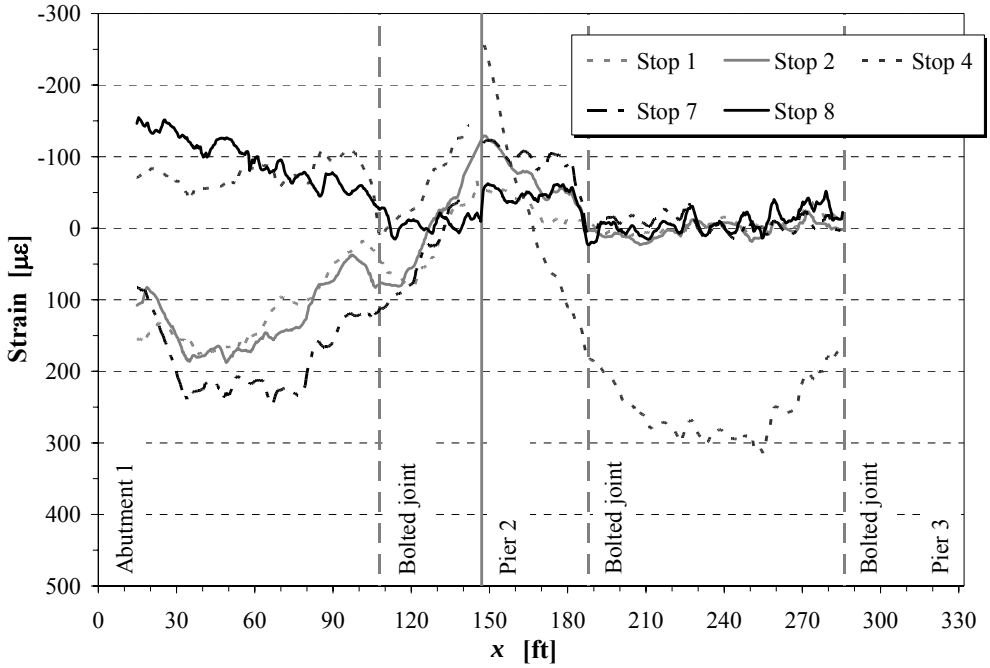

Girder 5 (Location C, Table 3.2)